P-061 High pressure NMR study of DHFR from a deep-sea bacterium

[1,2]Akihiro Maeno, [1,2]Sunilkumar P.N., [2]Hiroshi Matsuo, [3]Eiji Ohmae, [4]Chiaki Kato, [2]Kazuyuki Akasaka
[1]Grad. Sch. of Biol. Sci. and Tech, Kinki Univ., [2]HPPRC, Kinki Univ., [3]Grad. Sch. of Sci., Hiroshima Univ. [4]Inst. of Biogeosci., JAMSTEC

Prokaryotic life can adapt to extreme conditions such as low temperature and high pressure. Proteins are the key molecules of life and their structure and function must be adapted to extreme conditions. Protein function is closely related to its structural dynamics. Dihydrofolate reductase (DHFR) is an important enzyme involved in the reduction of dihydrofolate to tetrahydrofolate, which is a precursor for the biosynthesis of purines, pyrimidines and some amino acids (1).This enzyme is present in deep sea and terrestrial organisms. DHFRs from *Moritella profunda* (Mp, a deep sea bacterium) and *E.coli* (Ec, a terrestrial bacterium) show only 55% sequence similarity (**Figure 1)**. A comparison of the crystal structures of the two proteins show that the core structures of the two proteins are almost the same with some difference in the loop regions (**Figure 2**).

```
1RD7_A|PDBID|CHAIN|SEQUENCE      -MISLIAALAVDRVIGMENAMPWNLPADLAWFKRNTLDKPVIMGRHTWES
3IA5_A|PDBID|CHAIN|SEQUENCE      MIVSMIAALANNRVIGLDNKMPWHLPAELQLFKRATLGKPIVMGRNTFES
                                  ::*:***** :****::* ***:***:*  *** **.**::***:*:**

1RD7_A|PDBID|CHAIN|SEQUENCE      IGRPLPGRKNIILSSQPGTDDR-VTWVKSVDEAIAACGDVPEIMVIGGGR
3IA5_A|PDBID|CHAIN|SEQUENCE      IGRPLPGRLNIVLSRQTDYQPEGVTVVATLEDAVVAAGDVEELMIIGGAT
                                 ******** **:** *.. : . ** * ::::*:.*.*** *:*:***.

1RD7_A|PDBID|CHAIN|SEQUENCE      VYEQFLPKAQKLYLTHIDAEVEGDTHFPDYEPDDWESVFSEFHDADAQNS
3IA5_A|PDBID|CHAIN|SEQUENCE      IYNQCLAAADRLYLTHIELTTEGDTWFPDYEQYNWQEIEHESYAADDKNP
                                 :*:* *. *::******:  .**** *****  :*:.:  * : ** :*.

1RD7_A|PDBID|CHAIN|SEQUENCE      HSYCFEILERR-
3IA5_A|PDBID|CHAIN|SEQUENCE      HNYRFSLLERVK
                                 *.* *.:***
```

Figure 1: Sequence alignment between E.coli DHFR and Mp DHFR (CLUSTAL 2.1 multiple sequence alignment: 1RD7 – Ec DHFR and 3IA5 – Mp DHFR).

Keywords: High pressure NMR, Deep-sea enzyme, Pressure-adaptation

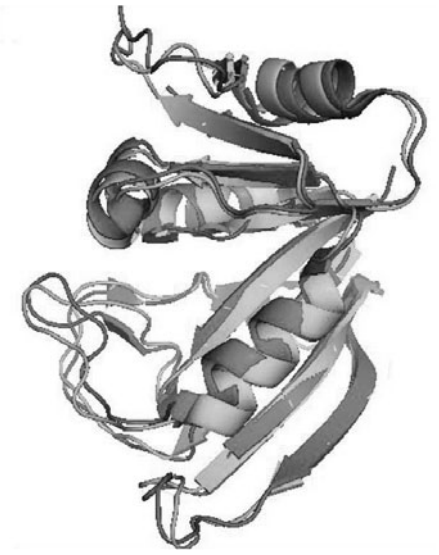

Figure 2: Superposition of Ec DHFR (PDB ID: 1RD7, Red) and Mp DHFR (PDB ID: 3IA5, Green)

Variable pressure 1D-^{1}H NMR study of these two proteins in the temperature range from -5 to 30°C show that the thermodynamic stability of Mp DHFR is less than that of Ec DHFR (2). A variable pressure 2D ^{1}H/^{15}N HSQC NMR study of Ec DHFR bound to folate show that the M20 loop is highly mobile and the open conformer has a population of ~20% under physiological conditions (3).

In order to understand the residue specific conformational fluctuations in Mp DHFR, we have done the sequence specific backbone resonance assignment. We have prepared a 2 mM solution of folate bound Mp DHFR. We have recorded the triple resonance spectra like HNCA, HNCOCA, HNCO, HNCACO, CBCANH and CBCACONH using the 600 MHz Bruker AVANCE spectrometer. Sequence specific backbone assignment has been done using the CCPNMR program. We are also reporting the residue specific conformational fluctuations of Mp DHFR protein using the variable pressure 2D ^{1}H/^{15}N HSQC spectra in the pressure range from 3 MPa to 300 MPa. A comparison of the results suggests how the conformational fluctuations are different in Ec DHFR (terrestrial) and Mp DHFR (deep sea). This may give some insight into the adaptation mechanism of proteins with external conditions and hence that of organisms.

References

1. M. R. Sawaya and, J. Kraut (1997). *Biochemistry*. 36: 586-603.
2. K. Hata, R. Kono, M. Fujisawa, R. Kitahara, Y. O. Kamatari, K. Akasaka and Y. Xu (2004). *Cell. Mol. Biol.* 50:311-316.
3. R. Kitahara, S. Sareth, H. Yamada, E. Ohmae, K. Gekko and K. Akasaka (2000). *Biochemistry*. 39: 12789-12795

P-062 Solution structure of ubiquitin fold domain in SUMO-activating enzyme E1 from rice: Structural differences in the binding region to SUMO-conjugating enzyme E2 play a critical role in E1-E2 specificity

Rintaro Suzuki, Wataru Tsuchiya, Heisaburo Shindo, Zui Fujimoto and Toshimasa Yamazaki
Biomolecular Research Unit, National Institute of Agrobiological Sciences

ABSTRACT

Post-translational modification of target proteins by SUMO regulates a wide variety of cellular functions. In the sumoylation process, an activated SUMO is transferred from an activating enzyme E1 to a conjugating enzyme E2. Among the multiple domains in E1, a C-terminal ubiquitin fold domain (UFD) shows highest affinity for E2. We determined NMR solution structure of UFD in rice E1. Comparison with crystal structures of UFD in other E1 enzymes for SUMO, ubiquitin and NEDD8, suggests that the variation in the UFD-E2 binding mode plays a critical role in determining E1-E2 specificity.

INTRODUCTION

Small ubiquitin-related modifier (SUMO) is a member of a protein family consisting of ubiquitin and ubiquitin-like proteins. Sumoylation is a post-translational modification and alters functions of many cellular proteins through changes in localization, activity, or stability. SUMO is first activated at its C-terminus by the SUMO-activating enzyme E1. SUMO E1 is a heterodimer composed of two subunits, SUMO-activating enzyme subunit 1 and 2 (SAE1 and SAE2). After thioester bond formation between the C-terminal carboxy group of SUMO and the catalytic Cys residue in SAE2, the thioester is transferred to the SUMO-conjugating enzyme E2. Finally, E2 transfers SUMO to the substrate protein, usually with assistance from SUMO E3 ligases. It has been proposed that E2 is recruited to the SUMO-E1 thioester-linked conjugate through its multiple binding sites or domains including the conjugated SUMO, the Cys domain of SAE2 with catalytic Cys residue, and the C-terminal ubiquitin fold domain (UFD) of SAE2. Among them, UFD showed the highest affinity for E2 and thus it was considered to play an essential role in SUMO transfer to E2.

There have been reported many crystal structures of UFDs of SUMO E1 (SAE2), ubiquitin E1 (ubiquitin-activating enzyme UBA1), and NEDD8 E1 (NEDD8-activating enzyme E1 catalytic subunit UBA3). However, no solution structure of UFD is available to date. Here we report a NMR solution structure of UFD of SAE2 from rice.

MATERIALS AND METHODS

Uniformly $^{13}C/^{15}N$-labeled UFD, comprising residues 436-550 of rice SAE2, was expressed as a GST-fusion protein in *E. coli* and purified by GSH-Sepharose column, followed by cleavage of the GST-tag and gel filtration chromatography. The recombinant protein thus obtained contains an additional amino-acid sequence of Gly-Pro-Leu-Gly-Ser at the N-terminus. Solutions used to record

SUMO-activating enzyme E1, Ubiquitin fold domain, SUMO-conjugating enzyme E2

NMR spectra contained the purified recombinant UFD (1.18-1.28 mM) dissolved in 10 mM potassium phosphate buffer, pH 7.0, with 100 mM NaCl and 10% $^{2}H_2O$.

All NMR spectra were acquired at 25 °C on a Bruker DMX 750 spectrometer equipped with pulse-field gradient. ^{1}H, ^{13}C, and ^{15}N sequential resonance assignments have been reported [1]. The spectra were processed using NMRPipe software and analyzed using SPARKY 3 software.

Interproton distance restraints for structural calculations were derived from multi-dimensional NOESY spectra with mixing times of 150 ms: 3D ^{15}N-separated NOESY-HSQC, 3D $^{13}C/^{15}N$-separated NOESY-HSQC, and 3D ^{13}C-separated NOESY-HSQC. Dihedral angle constraints of the main chain were obtained using the program TALOS+. Hydrogen bonds were assumed from the secondary structures determined from NOE patterns. Structural calculations were carried out using the program CYANA, version 2.1.

RESULTS AND DISCUSSIONS

The overall structure of UFD of rice SAE2 was similar to the X-ray crystal structures of UFD of human or yeast SAE2 (Fig. 1). It was also similar to the structures of the UFDs in human NEDD8-activating enzyme E1 catalytic subunit (UBA3) and in yeast ubiquitin-activating enzyme E1 (UBA1), except that the UFD of SAE2 has an additional β6-strand in the C-teminus. However, the length of secondary structural elements as well as the connecting loops varies throughout the domain. Particularly, the difference among α2-helices located on edge of the E2-binding region suggests considerable variations in interaction mode between UFD and E2.

UFD of human SAE2 showed two conformationa l states in the region K486-E499 comprising the Ubc9-binding surface. It was pointed out that this region is under equilibrium between minor unfolded conformer and major folded conformer containing β3-strand, and that such a conformational flexibility is important in the molecular recognition. In case of the UFD of rice SAE2, however, all residues were assigned uniquely in the ^{1}H-^{15}N HSQC spectrum and the conformational multiplicity was not observed. The structure of the rice UFD was well determined and the main-chain RMSD of calculated 20 structures was 0.29 for the whole protein other than the first five residues derived from the expression vector. The order parameters S^2 estimated by RCI indicated considerable flexibility of the short region in the loop connecting the β3-strand and α2-helix. Although the flexibility of the loop may take part in the E2 recognition in rice, the dynamic property of the recognition site of UFD seems different among species. The α2-helix in UFD of rice SAE2 is 11 residues long while that of the human SAE2 is a short 3_{10} helix. In respect to the length and the conformation, the α2-helix in the rice UFD resembles that in the human UBA3, which interacts with E2 directly.

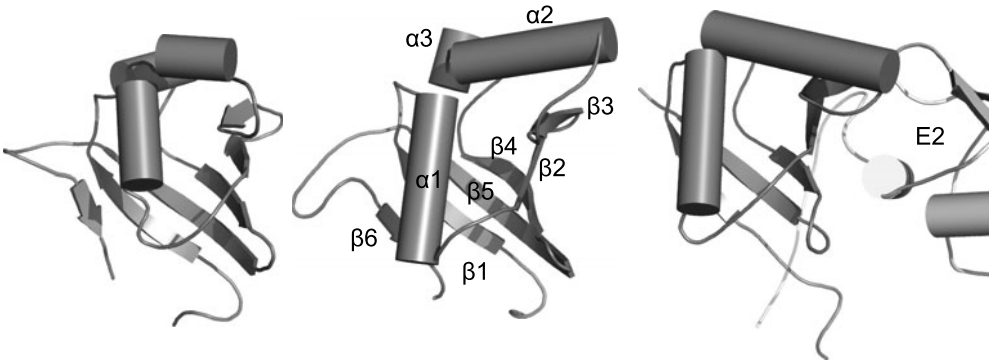

Figure 1 Comparison of UFDs

REFERENCE

1. Suzuki R. *et al.* (2011) Biomolecular NMR Assignments 5:245-248.

P-063 Impact of Charge Mutation on Equilibrium Binding and Encounter Complex Formation between the N-terminal Domain of Enzyme I and the Histidine Phosphocarrier Protein

Tae-kyung Yu, Ko On Lee and Jeong-Yong Suh

Biophysics and Nanobiology Laboratory, WCU Biomodulation Major, Department of Agricultural Biotechnology, Seoul National University, Seoul 151-921, Korea

ABSTRACT

Protein-protein association generally progresses toward the final well-defined stereospecific complex via the intermediary of a transient, lowly populated, encounter complex ensemble. Protein-protein interaction can be viewed as a two-step process comprising the initial formation of the encounter complex ensemble followed by rearrangement, along a two-dimensional energy landscape, to form the final stereospecific complex. The encounter complex formation has been reported between N-terminal Domain of Enzyme I (EIN) and the heat-stable histidine phosphocarrier (HPr) protein from bacterial phosphotransferase system.

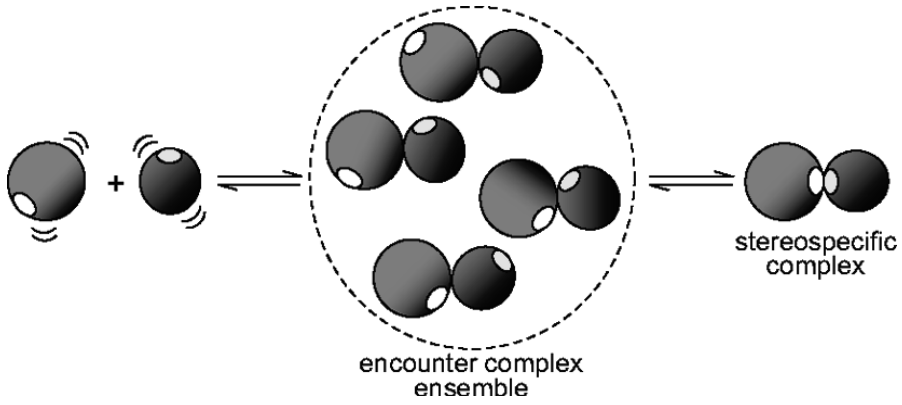

Figure 1. Protein-protein complex formation. The interaction surfaces involved in the stereospecific complex are shown in white and yellow.

Here, we investigated how charge mutations on the protein surface influence the encounter complex formation as well as the equilibrium binding using paramagnetic relaxation enhancement and isothermal titration calorimetry. We observed that perturbation of surface electrostatic potential away from the binding interface can change the equilibrium dissociation constant by changing the

distribution and/or population of the encounter complex ensemble. Monitoring the impact of different mutations on their thermodynamic binding and transient intermediate complex would be a useful tool to probe the target search process.

P-064 Functional Identification of Toxin-Antitoxin Molecules from *Helicobacter pylori* 26695 and Structural Elucidation of the Molecular Interactions Title

Sun Bok Jang[1], Kyung-Doo Han[1] and Bong-Jin Lee[1*]

[1] Research Institute of Pharmaceutical Sciences, College of Pharmacy, Seoul National University, San 56-1, Shillim-Dong, Kwanak-Gu, Seoul 151-742, Korea

ABSTRACT

Bacterial toxin-antitoxin (TA) systems are associated with many important cellular processes including antibiotic resistance and microorganism virulence. Here, we identify and structurally characterize TA molecules from the gastric pathogen, *Helicobacter pylori*. The HP0894 protein had been previously suggested, through our structural genomics approach, to be a putative toxin molecule. In this study, the intrinsic RNase activity and the bacterial cell growth-arresting activity of HP0894 were established. The RNA-binding surface was identified at three residue clusters: (Lys^{8} and Ser^{9}), (Lys^{50}–Lys^{54} and Glu^{58}), and (Arg^{80} and His^{84}–Phe^{88}). In particular, the -UA- and -CA- sequences in RNA were preferentially cleaved by HP0894, and residues Lys^{52}, Trp^{53}, and Ser^{85}–Lys^{87} were observed to be the main contributors to sequence recognition. The action of HP0894 could be inhibited by the HP0895 protein, and the HP0894-HP0895 complex formed an oligomer with a binding stoichiometry of 1:1. The N and C termini of HP0894 constituted the binding sites to HP0895. In contrast, the unstructured C-terminal region of HP0895 was responsible for binding to HP0894 and underwent a conformational change in the process. Finally, DNA binding activity was observed for both HP0895 and the HP0894-0895 complex but not for HP0894 alone. Taken together, it is concluded that the HP0894-HP0895 protein couple is a TA system in *H. pylori*, where HP0894 is a toxin with an RNase function, whereas HP0895 is an antitoxin functioning by binding to both the toxin and DNA.

Helicaobacter pylori, Toxin, Antitoxin

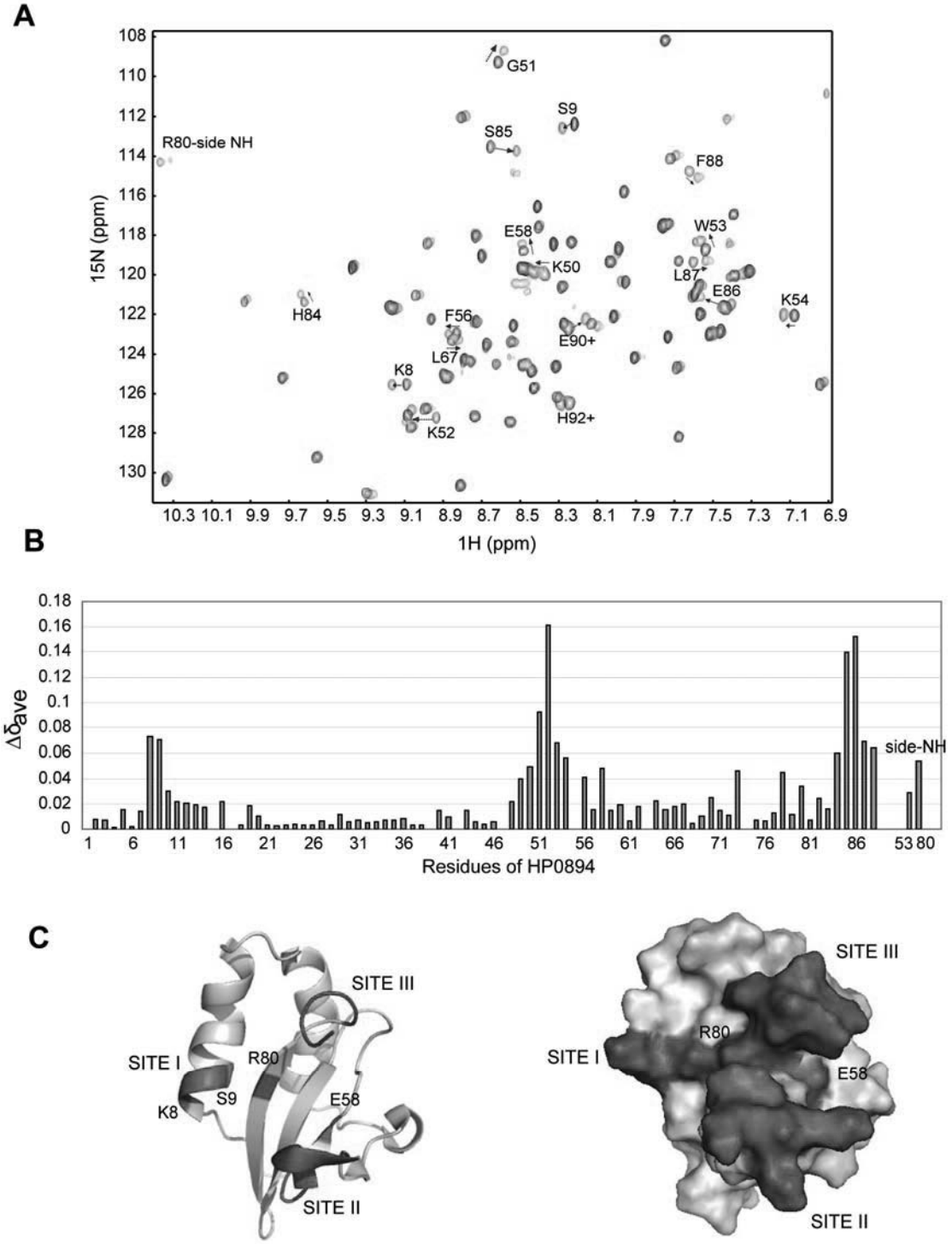

Figure 1. Chemical Shift Perturbation mapping of the ssDNA-U (d(ACACUAAGAA))-binding region on HP0894

P-066 Physicochemical Properties of Pyrazinamidase from *Mycobacterium tuberculosis*

Su-Jin Cho[1], Woo-sung Son[1], Won-Je Kim[1], & Bong-Jin Lee[1]

[1]Research 1Research Institude of Pharmaceutical Sciences,
College of Pharmacy,
Seoul National University, Kwanak-Gu, Seoul 151-742, Korea

ABSTRACT

Physicochemical properties of Pyrazinamidase (PncA), which activates antituberculosis drug pyrazinamide(PZA) by converting it into the active form, pyrazoic acid, were investigated. Structural information was obtained using circular dichroism (CD), nuclear magnetic resonance (NMR), homology modelling, and molecular dynamics (MD), enzymatic activity was measured according to Wayne's procedure, and enzyme kinetic parameters were carried out by one-dimensional NMR experiment. PncA is an Mn^{2+}/Fe^{2+} -containing protein with a molar ratio of $[Mn^{2+}]$ to $[Fe^{2+}]$ of 1: 1. The metal binding states of PncA were determined by Inductively Coupled Plasma-Mass Spectroscopy. Ten PncA mutants were generated by site-directed mutagenesis. H57A among these mutants, the essential residue for metal ion binding, showed significant data of two dimensional NMR experiments. The results of study implicate that aromatic residues in active site lead to unique feature of *M. tuberculosis* PncA with regard to hydrolysis and metal coordination and this feature is related to PZA-resistance mechanism in TB

Pyrazinamidase, Mycobacterium tuberculosis, NMR

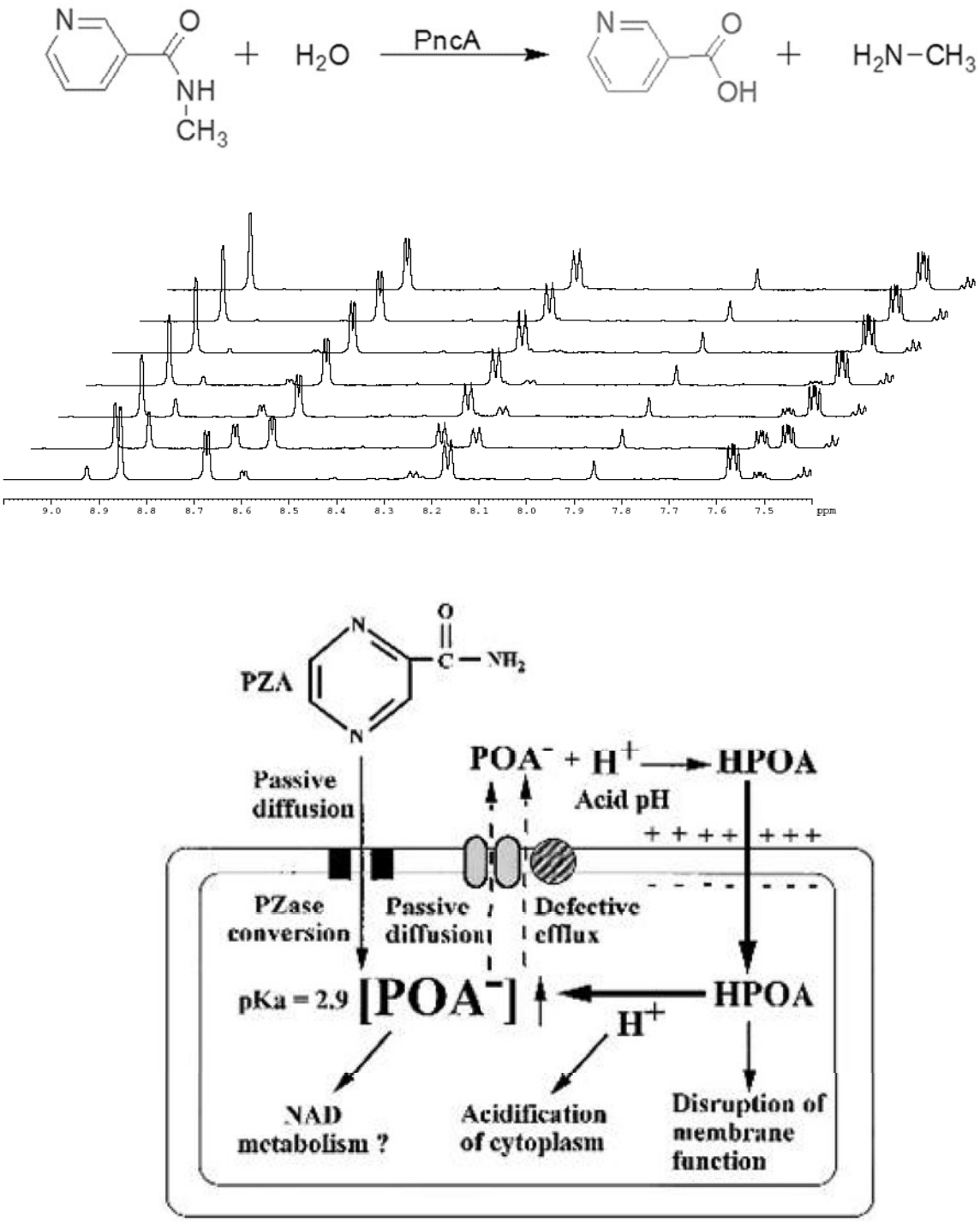

Figure 1. Mechanism of action of PZA on *Mycobacterium tuberculosis*

P-067 NMR solution structure of HP0827 (O25501_HELPY) from Helicobacter pylori: model of the possible RNA-binding site

Yeon-Jin Yang[1], Sun-Bok Jang[1], and Bong-Jin Lee[1*]

[1] Research Institute of Pharmaceutical Sciences, College of Pharmacy, Seoul National University, San 56-1, Shillim-Dong, Kwanak-Gu, 151-742, Korea

ABSTRACT

The HP0827 protein is an 82-residue protein identified as a putative ss-DNA-binding protein 12RNP2 Precursor from Helicobacter pylori. Here, we have determined 3D structure of HP0827 using Nuclear Magnetic Resonance. It has a ferredoxin-like fold, beta1-alpha1-beta2-beta3-alpha2-beta4 (alpha; alpha-helix and beta; beta-sheet) and ribonucleoprotein (RNP) motifs which are thought to be important in RNA binding. By using structural homologues search and analyzing electrostatic potential of surface, we could compared HP0827 with other RNA-binding proteins (sex-lethal, T-cell restricted intracellular antigen-1, U1A) to predict RNA-binding sites of HP0827. We could predict that beta sheets of HP0827, especially beta1 and beta3, are primary region for RNA binding. Consequently, similar to other RNA-binding proteins, RNP motifs (Y5, F45, F47), positively charged and hydrophobic regions (K32, R37, K40, K41, K43, R70, R73) are proposed as a putative RNA-binding sites. In addition, differences in amino acids composition of RNP motifs, N, C-terminal residues, loop-region fold and the orientation of alpha1-helix with other RNA recognition motif proteins could give specific biological functions to HP0827. Finally, the study on natural RNA target is also important to completely understand the biological function of HP0827.

Helicobacter pylori, RRM, RNP

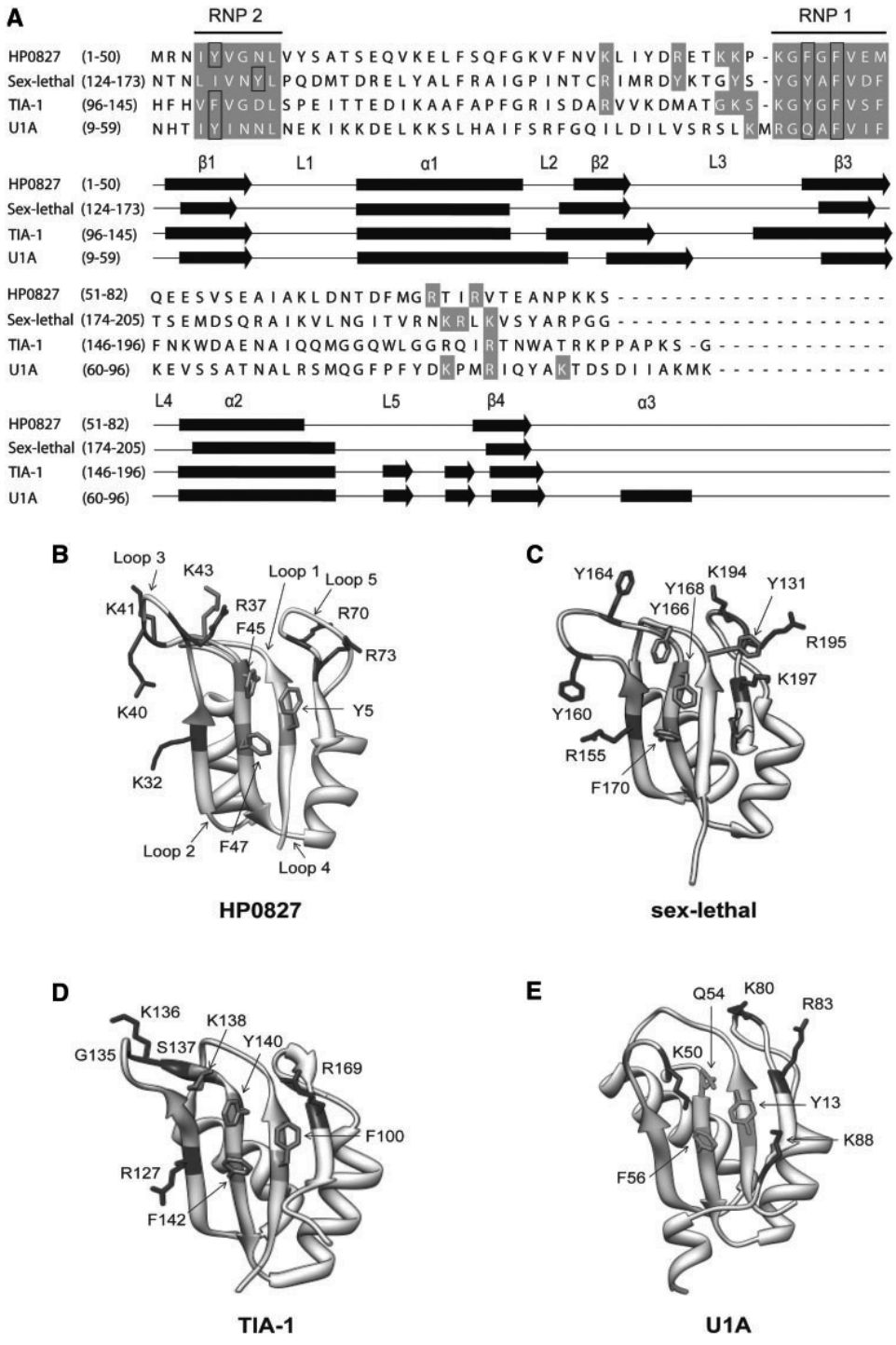

Figure 1. Sequence Alignment and comparison of structural homologues of HP0827

P-068

Solution structure of hypothetical protein HP1423 (Y1423_HELPY) reveals the presence of aL motif related to RNA binding

In-gyun Lee, Ji-Hun Kim, Sung Jean park, Ki-Young Lee, Woo-Sung Son, Na-Young Sohn, Ae-Ran Kwon, and Bong-Jin Lee[1]

[1]Research Institute of Pharmaceutical Sciences, College of Pharmacy, Seoul National University, Kwanak-Gu, Seoul 151-742, Korea

ABSTRACT

Helicobacter pylori has uniqueness to survive in the extreme acidic environment in stomach. It is an important human bacterial pathogen, causing diverse gastric diseases such as peptic ulcers, chronic gastritis, and mucosa-associated lymphoid tissue lymphoma. In addition, the fact that duodenal ulcers are also associated with H. pylori infection has been proposed. H. pylori was isolated from human stomachs in 1979 for the first time, and whole-genome analysis of H. pylori was completed in the United States in 1997. Until now, complete genome sequences for the H. pylori strain 26695, J99 and HPAG1 have been determined. Even though the genomic information is known well, the functions of many genes are still unknown. The functional studies are still required to expand our biological understanding for H. pylori. In this regard, determining three-dimensional structures of unknown proteins can lead to the elucidation of biological function of proteins and the discovery of new drug target candidate for antibiotics. In this study, we determined the solution structure of HP1423 (Y1423_HELPY), which has 84 amino acid residues, conserved hypothetical protein from H. pylori strain 26695. According to Pfam database, HP1423 belongs to S4 (PF01479) superfamily. The S4 domain is a small domain consisting of 60–65 amino acid residues that probably mediates binding to RNA. The structure of HP1423 revealed the presence of the aL-RNA binding motif in the protein, which is a general feature of several RNA binding protein families.

Helicobacter pylori, NMR, HP1423

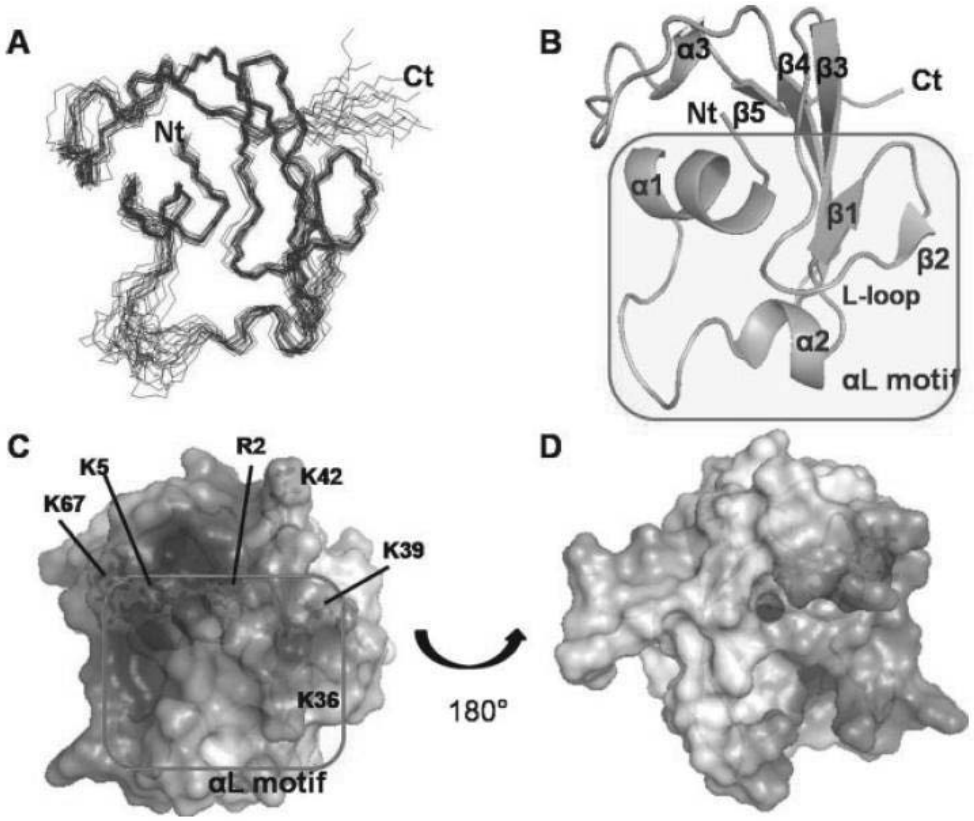

Figure

NMR solution structure of HP1423. A: The superposition of the final 20 structures over the energy-minimized average structure. B: Ribbon drawing of the representative conformer of HP1423. C, D: Electrostatic potential surface diagrams of HP1423 orientated to show the proposed RNA-binding aL motif facing outwards. The extreme ranges of red (negative) and blue (positive) represent electrostatic potentials of less than 29 to greater than 19 kbT, where kb is the Boltzmann constant and T is the temperature. The figure was calculated with APBS15 showing the accessible surface.

P-069 Fitting the puzzle together: the cage complexes with an encapsulated cobalt(II) ion as new paramagnetic tags

Valentin Novikov, Andrey Lebedev, Yan Voloshin
Nesmeyanov Institute of Organoelement Compounds RAS, Moscow, Russia

Macrobicyclic tris-dioximate complexes with an encapsulated cobalt(II) ion are perspective paramagnetic labels owing to the complete isolation of a paramagnetic ion and hence the stability of the complex and the independence of its magnetic characteristics from the environment. The pseudocontact interactions with the cobalt(II) ion lead to the paramagnetic shift of distant (>2.5 nm) nuclei signals in NMR spectra, paving the way for the use of the cobalt(II) cage complexes as non-covalent paramagnetic tags.

Hyperfine shifts in NMR spectra of paramagnetic ion's complexes provide a wealth of information about the structure and dynamics of the investigated molecules [1]. The paramagnetic tags containing lanthanide or *d*-group metal ions are nowadays broadly used for structural characterization of complex biological systems. Macrobicyclic tris-dioximate complexes with an encapsulated cobalt(II) ion (Fig. 1) are perspective paramagnetic labels owing to the complete isolation of the metal ion [2]; hence the stability of the complex and its magnetic characteristics do not depend on the environment. The functionalization of such complexes by six ribbed and two apical substituents gives a room for fine tuning the characteristics of an encapsulated ion to achieve the desired features.

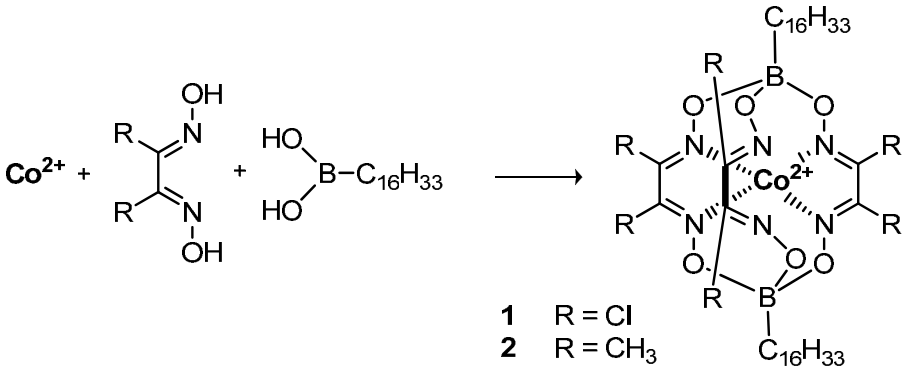

Fig. 1. Clathrochelate complexes **1** and **2**

The ^{1}H NMR spectra of $C_{16}H_{33}$-substituted hexachlorine-containing cobalt(II) clathrochelate (Fig. 2A) provide an example of significant downfield pseudocontact shifts, leading to a complete resolution of the fifteen signals of methylene group's protons, otherwise heavily overlapped. The influence of the paramagnetic center can be detected at the distance exceeding 2.5 nm, suggesting the large anisotropy of the magnetic susceptibility.

At the same time, the complex **2**, which differs from **1** by six methyl ribbed groups, give rise to a completely diverse spectrum (Fig. 2B). The signals of long-chain aliphatic substituent show small upfield paramagnetic shifts. The reversion of the direction of the shift provides evidence of the completely different electronic structure of **1** and **2**.

The NMR spectra, combined with EPR and magnetochemical data, show that the choice of dioximate ribbed groups affects tremendously the magnetic properties of an encapsulated ion, enabling the spin transition in these complexes. Those in a low-spin state demonstrate dynamic Jahn-Teller distortion [3], which results in the shift of an encapsulated cobalt(II) ion from the center of the macrobicyclic ligand's cavity, while the high-spin complexes have a C_3 symmetry.

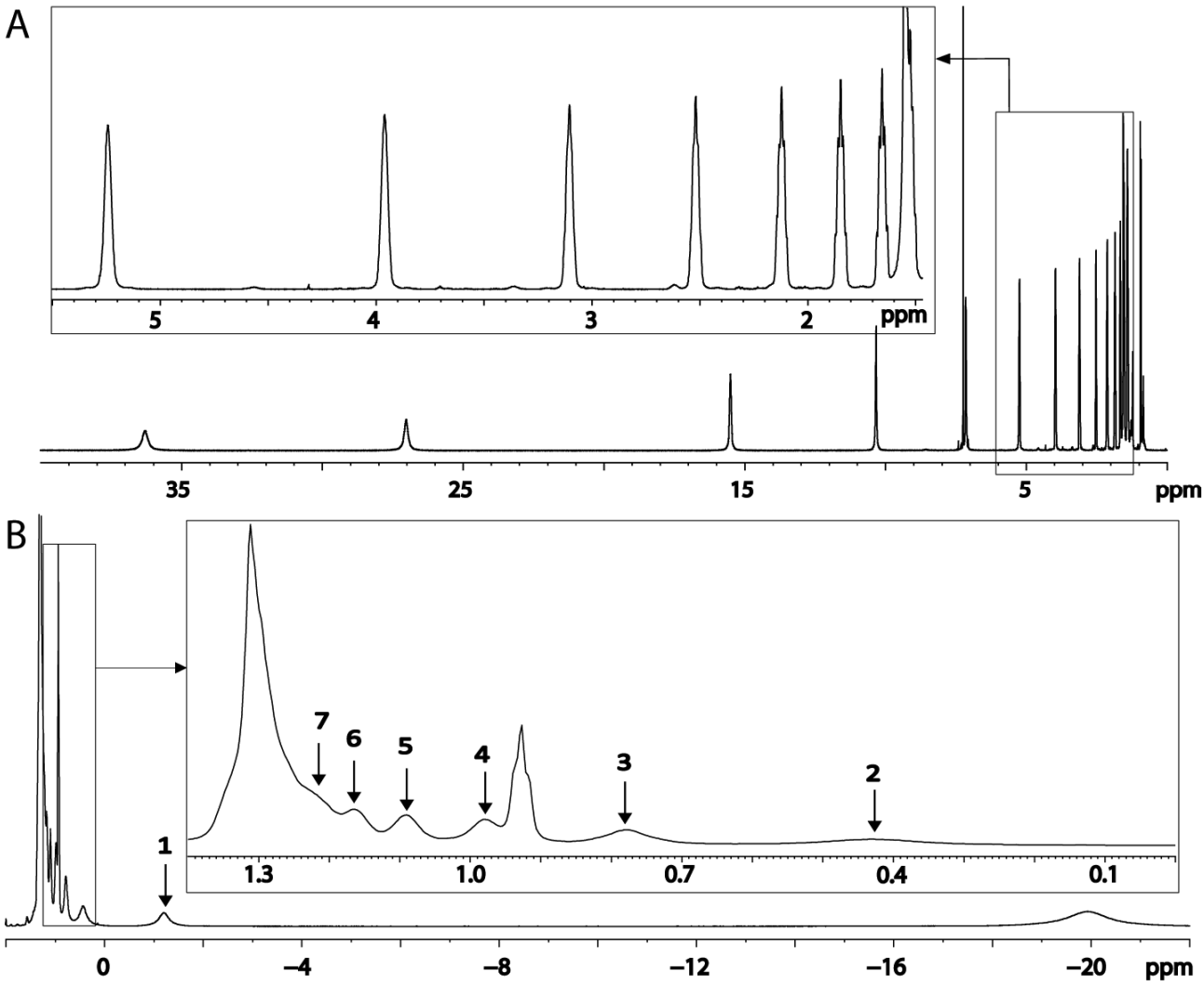

Fig. 2. The ^{1}H NMR spectra of clathrochelate complexes (A) **1** and (B) **2**.

The different magnetic properties of these complexes suggest two separate areas for their application: the high-spin complexes can be used as the shifting agents, and the low-spin complexes as the relaxing agents.

Acknowledgements: The study was supported by Russian Foundation for Basic Research (10-03-00837) and Council of the President of the Russian Federation for young scientists support (MK-3161.2010.3).

References:

[1] Bertini I., Luchinat C., Parigi G., Solution NMR of paramagnetic molecules - applications to metallobiomolecules and models, Elsevier, Amsterdam (2001).

[2] Voloshin, Y.Z., Varzatskii, O.A., Vorontsov, I.I., Antipin, M.Y., *Angew. Chem. Int. Ed*., **44**, 3400-3402 (2005).

[3] Voloshin Y.Z. , Varzatskii O.A., Novikov V.V., Strizhakova N.G., Vorontsov I.I., Vologzhanina A.V., Lyssenko K.A., Romanenko G.V., Fedin M.V., Ovcharenko V.I., Bubnov Yu.N.,, *Eur. J. Inorg. Chem.*, **34**, 5401-5415 (2010).

Paramagnetic tags, pseudocontact shift, cage complexes

P-070 Sampling technique for physicochemical analysis of the hydrosphere detritus and benthos

Taiga Asakura[1], Seiji Yoshida[1], Yasuhiro Date[1, 2] and Jun Kikuchi[1, 2, 3, 4]

[1]Grad. Sch. Bionano Sci., Yokohama City Univ. , [2]RIKEN Plant Science Center, [3]RIKEN Biomass Eng. Prg. and [4]Grad. Sch. Bioagri., Nagoya Univ.

The detritus cycle has an important role in ecosystem including the particle self-organization of polysaccharides and their degradation. In addition, rich detritus is formed in the estuarine region by tidal action and contributes to the water purification or marine resources. We examined the sampling technique for elucidation of metabolism in the hydrosphere detritus and benthos. The metabolic profiles both detritus and benthos showed environmental dependent feature.

[Introduction]

Ecosystem services are precious and irreplaceable for human life, especially the estuarine environment is known as highest value among various natural ecosystems. The basic structure of the estuarine ecosystems is mainly composed of nutrients, phytoplankton, zooplankton, benthos, fish and detritus (Fig. 1). The detritus is a particulate organic matter (POM) as opposed to dissolved organic matter (DOM). The detritus is typically derived from the bodies or fragments of dead organisms as well as fecal material. In addition, many microbes propagate around the detritus and greatly contribute to the material cycles in the estuarine ecosystems. In estuarine ecosystems, however, relationships between variations of chemical compositions in fishes and the detritus profiles reflected to the environmental changes in their habitats are not extensively studied. Therefore, evaluation and characterization of the detritus profiles as well as variations of chemical compositions in fishes is a significant challenge to monitor the estuarine ecosystems.

Our objective of this study is to develop a sampling technique for physicochemical analysis of the hydrosphere detritus and to elucidate the relationships between metabolic profiles in fishes and the detritus profiles by NMR-based metabolomics approach. To this end, we focused on the evaluations for detritus profiles in estuarine sediment and metabolic profiles in *Gobiidae* Spp. who are primary consumers of the estuarine ecosystem in the Keihin area in Japan to develop and establish the sampling methodology for monitoring in the estuarine environment. We examined the POM sampling and extraction method from detritus by based on NMR spectral patterns. Therefore, detritus from the estuarine sediments were sampled, and here showing preliminary investigation of these NMR-based metabolic profiling.

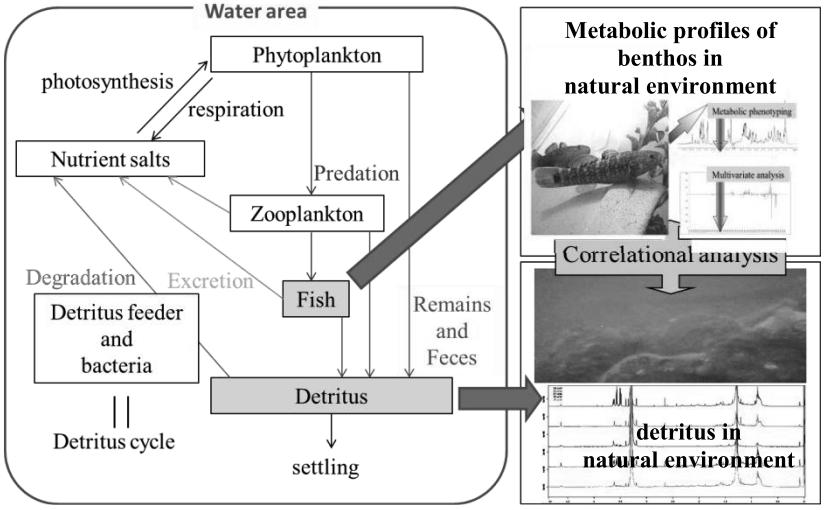

Fig. 1: The basic structure of the estuarine ecosystem

Keyword: metabolomics, detritus, hydrosphere

[Material and Methods]

To mine environmental information in individual estuarine ecosystem by evaluation of the metabolic profiles in fish, we collected a muscle part of the gobies that we sampled from the different estuarine regions such as Tsurumi River, Tama River, Arakawa River and Sagami River. The freeze-dried muscle sample was crushed by a food mixer and was extracted using KPi buffer for NMR measurements. The NMR data were processed by binning, digitizing and evaluating with multivariate statistical analysis such as principal components analysis (PCA).

For development and establish the sampling technique for physicochemical analysis of the hydrosphere detritus, we chose the spot that became the tidal flat in Tsurumi River estuarine as the main target ground of the sampling. The samples were also obtained from the mud (the lower layer and the surface layer) in the Tsurumi River on August 13, 2011, the mud at the Aburatsubo coast on August 15, 2011, the soils of the neighborhood and the mud (the surface layer) in the Tsurumi River on July 29, 2011. The extraction methods we examined were as follows. At first, the collected mud and soils were freeze-dried. The samples were suspended in a solvent in 2 ml of tubes and were incubated with shaking at 50 ºC for 15 min in order to extract the metabolites. After incubation and extraction process, the supernatants were measured by NMR spectroscopy. In this study, we examined the solvents of KPi, MeOD, DMSO-d_6, $CDCl_3$ and HFA▪$3D_2O$ with EDTA-d_{16}. In addition, we experimented about the filtering method.

[Results and Discussion]

Although our sampled gobies were three kinds of species and sex difference, overall metabolic profiles did not differ, but clarified by environmental factors. For example, PCA score plots showed distinguishable metabolic profiles between Sagami River and others (Fig. 2). This observation was likely to be caused by the differences that the Sagami River exhibit relatively pure water, whereas other rivers are muddy. In addition, data spots from Tsurumi River approached those from Tama River, reflecting that these rivers are at the geographically near position.

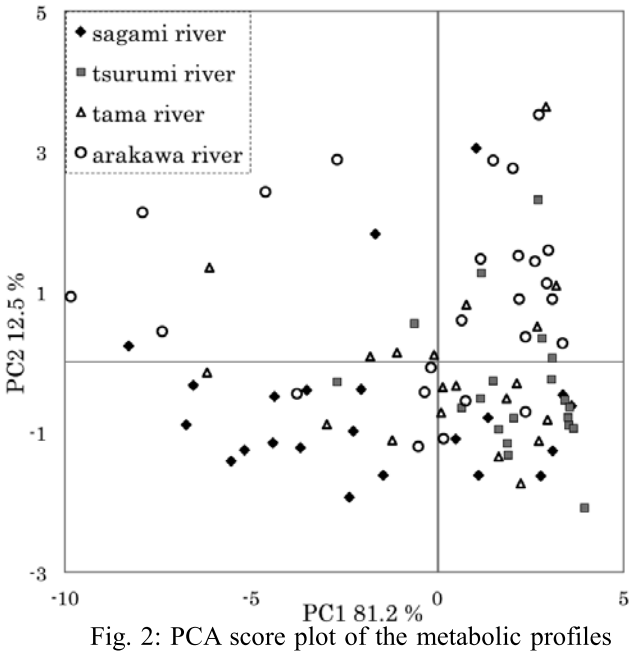

Fig. 2: PCA score plot of the metabolic profiles of the goby muscles sampled from four rivers.

On the other hand, investigation of extraction solvent for detritus often showed unusual spectra. However, use of MeOD solvent exhibited reasonable narrow line width with a plenty of metabolites, like we examined using wide range of organisms[1]. We observed sampling point-dependence of overall spectral pattern than the sampling time-dependence from same points.
Therefore, we obtained environmental dependence of the metabolic profile from both gobies and detritus. We will next perform correlation analysis between them.

Reference:

1) Sekiyama, Y., Chikayama, E. and Kikuchi, J. “Evaluation of a semipolar solvent system as a step toward heteronuclear multidimensional NMR-based metabolomics for ^{13}C-labeled bacteria, plants, and animals” *Anal. Chem.* **83**, 719-726 (2011).

P-071 Thermal isomerization and paramagnetic relaxation of poly(n-propyl propiolate)

Takenori Shibayama[1], Shu Arahi[1], Yasuteru Mawatari[2], Masayoshi Tabata[2],and Toshifumi Hiraoki[1]
[1]Hokkaido University, Graduate School of engineering,
[2]Muroran Institute of Technology

Abstract

The temperature dependence of ^{1}H and ^{13}C NMR spectra, relaxation times and ESR spectra were investigated in order to study the conformation and the paramagnetic effect of Poly(n-propyl propiolate) in tetrachloroethane. ^{1}H and ^{13}C NMR spectra and T_2 values on the polymer were found to change remarkably at above 70˚C, but T_1 values were almost constant, showing the paramagnetic interactions. Radical concentration on the polymer increased at above 80˚C. The polymer in solution thermally isomerizes and simultaneously produces radicals.

1. Introduction

Poly(n-propyl propiolate)(PnproP) with a stereoregular structure shows the cis-transoid to trans-transoid isomerization, and simultaneously produces radicals on the chain with increasing temperature in solid[1]. In this work, we measured the temperature dependence of ^{1}H and ^{13}C NMR spectra, relaxation times of the polymer in tetrachloroethane, and discussed conformation of the polymer and paramagnetic effects in solution.

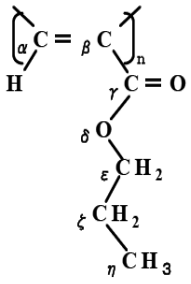

Scheme1 PnproP

2. Measurements

PnproP was prepared by the reported method[2].^{1}H and ^{13}C NMR spectra and T_1, T_2 value were measured on Bruker DSX-300(300.13MHz). T_1 value was measured by inversion recovery, and T_2 value was obtained by the half width and CPMG. ESR spectra were recorded on a JEOL FE1X(9.2GHz).

3. Results and discussion

The radical concentration on the polymer obtained from ESR measurements is shown in Fig.1. The number of the residue of the polymer per a spin was about two hundred thousand below at 50˚C, and increased abruptly at above 85˚C and reached about four thousand.

The main chain H_α signal of ^{1}H NMR spectra of PnproP is shown in Fig.2. With increasing temperature, H_α signals became broader and new broad signals were appeared around of the sharp H_α signal. Such broadenings of resonances were observed for other ^{1}H and ^{13}C signals of PnproP, including the methyl group in the end of sidechain. And these effect were found to depend on the position of nuclei on the polymer, especially the distance between the

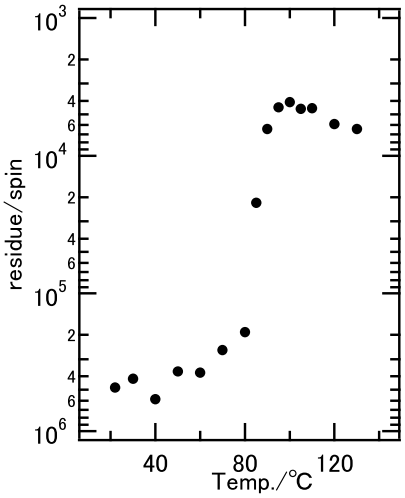

Fig.1 Temperature dependent radical concentration.

main and side chain. These results are caused by the paramagnetic interactions between nuclei and radicals in the high temperature region. Since there is one electron on about 4000 residues and no sharp signal of H_α signal above 80˚C, radicals produced are judged to delocalize on the chain.

Fig.3 shows temperature dependent chemical shift values of H_α. The closed circle corresponds to the first heating process and the open circle the second heating process of the annealed sample. In the first heating, the chemical shift value of H_α became slightly larger with increasing temperature, and at around 75˚C it suddenly changed about by 0.05ppm larger. In the second heating, the broad H_α signals were only observed and their temperature dependence of chemical shift values was opposite to that in the first heating process, suggesting that their deviations correspond to the paramagnetic shift and follow to Curie's law.

Fig.4 shows temperature dependent T_1 and T_2 values of H_α signal. In the low temperature region of below 70˚C, $1/T_1$ and $1/T_2$ values decreased with increasing temperature. At the isomerization temperature of around 80˚C $1/T_2$ values increased abruptly by ten times while $1/T_1$ values were almost constant. These results indicate new paramagnetic relaxation processes due to radicals contribute to T_1 and T_2 values. As $1/T_2$ values are much larger than $1/T_1$ values, Fermi contact interaction contributes to the T_2 process. This interaction was found to exert on the end of the side chain. We will make a presentation more quantitative discussion of chemical shifts and relaxation times.

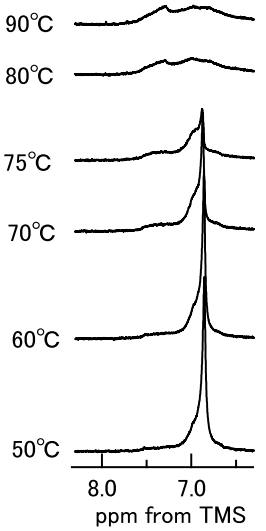

Fig.2 Temperature dependent H_α spectra.

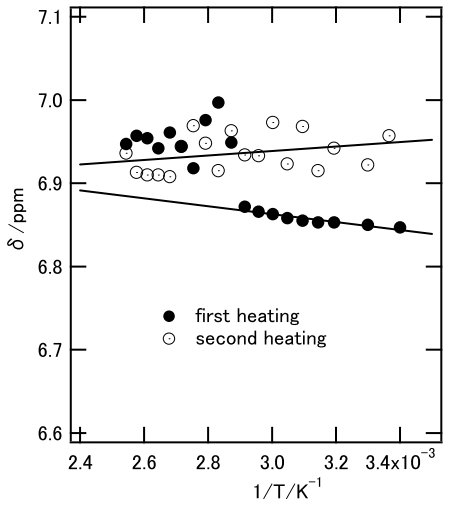

Fig.3 Temperature dependence of H_α chemical shift values.

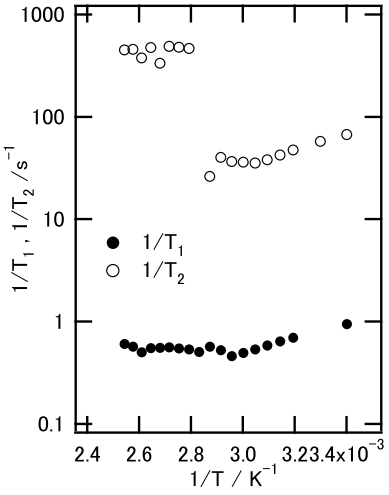

Fig.4 Temperature dependent relaxation times of H_α signal.

Reference

[1] M. Tabata, et al., *Macromolecules*, *27*, *6234* (1994)

[2] M. Tabata, et al, *J. Polym. Sci., Polym. Chem., 36,* 2457 (1998).

Keywords: poly-propiolate, thermal isomerization, paramagnetic relaxation

P-072 ^{13}C-NMR analysis for the quantitative observation of rapid proton exchange on LewisX hydroxyl groups in water

Shinya Hanashima[1], Koichi Kato[2,3] and Yoshiki Yamaguchi[1]
[1]Structural Glycobiology Team, RIKEN ASI
[2]Department of Structural Biology and Biomolecular Engineering, Nagoya City University
[3]Okazaki Institute for Integrative Bioscience and Institute for Molecular Science, National Institutes of Natural Sciences

Introduction

Hydroxyl protons of glycans play key roles in intermolecular interactions by forming hydrogen-bond networks. However, the fast exchange property of the sugar hydroxyl protons with surrounding water molecules has disturbed their observations by NMR.

Deuterium secondary isotope shifts on ^{13}C-chemcal shifts (DIS) of the sugar molecules have been observed at the geminal ^{13}C-signal of exchangeable hydroxyl protons (Fig. 1). The properties have allowed the ^{13}C-NMR signal shape to be used as a good indicator of low energy barrier hydrogen bonds.[1]

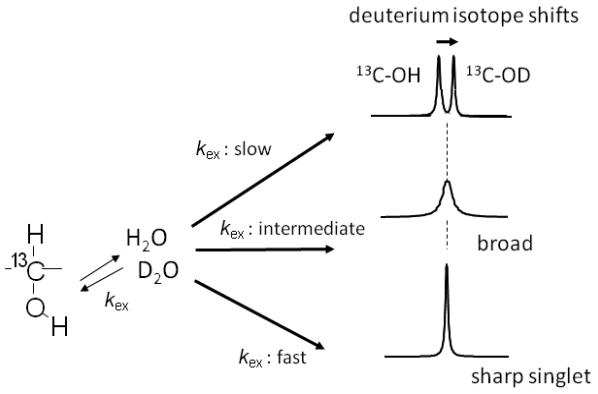

Fig 1. ^{13}C-NMR isotope shifts for analyzing the proton exchange rate of sugar hydroxyl groups. k_{ex}; exchanging rates of hydroxyl protons. The chemical shifts difference is ~0.15 ppm

LewisX **1** is involved in initial cell-cell interactions by forming a LewisX-Ca^{2+} complex. However, there is no consensus about the spatial atomic-arrangements of the LewisX-Ca^{2+} complex in water, and progress has been hampered by its weak binding (K_d = several hundred mM to several M) and dynamic nature. Here we use DIS of ^{13}C-NMR to analyze a LewisX interaction by observing sugar hydroxyl protons in the presence of Ca^{2+}.[2]

Results and Discussion

We initially investigated the effect of Ca^{2+} in the LewisX-LewisX interaction through titration experiments, monitored by ^{1}H-^{13}C HSQC chemical shift perturbations. However, the results indicated non-specific binding and we could not identify the specific groups involved in the LewisX-LewisX interaction. In contrast, we obtained the data suggestive of a LewisX- LewisX interaction when we analyzed the interaction by deuterium isotope shifts through evaluating proton exchange rates of the sugar hydroxyl groups.

^{13}C-NMR spectra were collected at temperatures from −10 °C to 20 °C in 5 °C increments. The synthetic LewisX trisaccharide **1** (40 mM) was dissolved in H_2O/D_2O = 50:50 solution with 1.0 M $CaCl_2$ (pH 6.0), and representative ^{13}C-NMR spectra at 5 °C are shown in Fig. 2b. DIS based on the β-shifts of ^{13}C-signals originating from FucC2, FucC4, GalC2, GalC4, GalC6 and GlcNAcC2 were observed. In contrast, ^{13}C-NMR spectra collected without $CaCl_2$ provided sets of DIS signals originating from GalC4 and GlcNAcC2 (Fig. 2a). Thus C2 and C6 of Gal, and C2 and C4 of Fuc provide DIS only in the presence of Ca^{2+}. In sharp contrast, the use of monosaccharide units,

either β-(OMe)-galactoside or α-(OMe)-fucoside, does not exhibit any significant signal change. To analyze proton-exchange under more restricted exchange conditions, we collected ^{13}C-NMR spectra at −10 °C using a 3 mm NMR tube. Now DIS were additionally observed from GalC3, FucC3 and GlcNAcC6, and only in the presence of 1.0 M $CaCl_2$ (Fig. 2c, 2d). Furthermore, ^{13}C-signals originating from GalC2, GalC3 and FucC3 show complicated splitting patterns because of the γ-shifts (0.005-0.02 ppm) arising from vicinal slow-exchanging protons at hydroxyl functionalities. These results suggest that Ca^{2+} participates in the LewisX trisaccharide complex formation, but has no effect on the monosaccharide components of LewisX. Furthermore, it is evident that all of the C-OH residues that exhibit DIS signals are directly or indirectly involved in the LewisX-LewisX interactions.

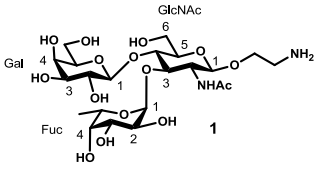

The proton exchange rates of the hydroxyl groups, which express the isotope-shifts, are estimated by applying each deuterium isotope shift to Gutowski's equation. The coalescence temperature of the ^{13}C-signals originating from GalC2, GalC6, FucC2, FucC3 and FucC4 is elevated more than 10 K in the presence of 1.0 M $CaCl_2$. Stabilization of these hydroxyl protons suggests that they play a significant role in LewisX-Ca^{2+} complex formation due to their forming inter- and intra-molecular hydrogen-bond networks with neighboring hydroxyl groups or through coordination with Ca^{2+}. In addition, GalC4 shows a partial increase in proton exchange, which might be due to disrupting their hydrogen bonding network.

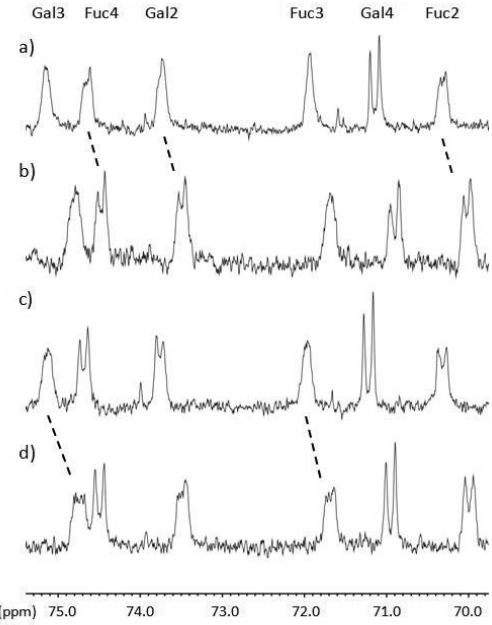

Fig 2. ^{13}C-NMR spectra of 40 mM LewisX with expanded secondary carbon area. LewisX at 5 °C a); LewisX with 1.0 M $CaCl_2$ at 5 °C b); LewisX at −10 °C c); LewisX with 1.0 M $CaCl_2$ at −10 °C d).

Conclusion

We describe a ^{13}C-NMR technique that analyzes LewisX-LewisX interactions through measurement of proton-exchange rates under physiological conditions. The technique is able to quantify the proton exchange of hydroxyl groups on glycans in 100% water, in the ten to hundred milliseconds range. It revealed that Ca^{2+} slows the rates of H/D exchange of several hydroxyl protons of LewisX. These groups must be involved in the LewisX-LewisX interaction. Our approach not only observes hydroxyl protons but also precisely evaluates their dynamics through measurement of the small difference in their exchange rates. This simple ^{13}C-NMR strategy is suitable for analyzing extremely weak interactions including those between carbohydrates, and identifies the hydroxyl protons involved in hydrogen bonding.

References

1. K. Uchida, J. L. Markley and M. Kainosho, *Biochemistry*, **2005**, *44*, 11811-11820.
2. S. Hanashima, K. Kato, Y. Yamaguchi, *Chem. Commun. in press*.

Hydroxyl proton, ^{13}C-NMR, glycan

P-073 Selective COSY-J-resolved-HMBC, A New Method for Improving Sensitivity of Cross Peaks of Methine Proton Signals Attached to A Methyl Group in J-resolved HMBC or Selective J-resolved HMBC

Kazuo Furihata

Division of Agriculture and Agricultural Life Sciences, University of Tokyo

We present an improved version of the J-resolved HMBC or Selective-J-resolved-HMBC technique named Selective COSY-J resolved HMBC. This method enables to improve the sensitivity of cross peaks of methine proton signals attached to a methyl group in J-resolved HMBC[1] or Selective J-resolved HMBC[2]. Natural products such as polyketides often contain spin systems which include a methine group (-CH-CH(CH_3)-CH-). In such a spin system, methyl protons split into a doublet with strong signal intensity. Therefore, methyl proton signals give cross peaks with stronger intensity as compared with those of methine protons in the J-resolved HMBC or Selective-J-resolved HMBC spectra.

On the other hand, a methine proton connected to a methyl group splits to a multiplet by surrounding several vicinal protons causing weak appearance of the methine proton signal. Therefore, it becomes difficult to observe long range J_{CH} cross peaks of the methine proton in the J-resolved HMBC or Selective J-resolved HMBC spectra. In order to solve this problem, we have developed a new technique, Selective COSY-J-resolved-HMBC(Fig.1). The key point of this method is to transfer the magnetization of a methyl group to its adjacent methine proton.

This Selective-COSY-J-resolved-HMBC method consists of a combination of the 1D-COSY and Selective J-resolved HMBC methods. Selective J-resolved HMBC is a selective version of J-resolved HMBC.

The 1D-COSY pulse is used for transfer of the proton magnetization from a methyl group to its adjacent methine proton. For a selective excitation pulse in the 1D-COSY method, selective 90 pulse is employed as the initial 90 pulse.

$$90x(sel) - \triangle/2 - 180x - \triangle/2 - 90y$$

Several methyl groups with similar chemical shifts can be activated simultaneously by selective excitation of the methyl group.

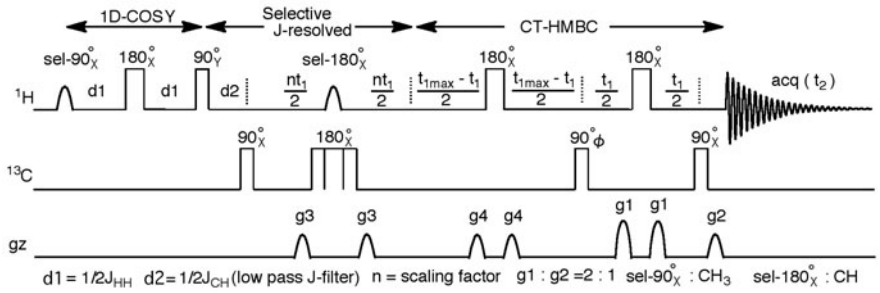

Fig.1 Selective COSY-J-resolved HMBC pulse sequence.

J-resolved HMBC, Selective J-resolved HMBC, Selective COSY-J-resolved HMBC

Selective COSY-J-resolved-HMBC spectra of portmicin (Fig. 2)

In Fig. 2, tow spectra of (a) Selective J-resolved HMBC and (b) Selective COSY-J-resolved-HMBC-1 of portmicin are shown. Projection of these spectra show that the selective COSY J-resolved HMBC-1 spectrum is higher in sensitivity than the Selective J-resolved HMBC spectrum.

In Selective COSY-J-resolved HMBC-1 spectrum, all proton-proton spin couplings of F1-dimension of 4-H are decoupled, and lengthwise cross peaks are observed. In addition, the cross peaks that split by long range J_{CH} are observed as a doublet. The value of long range J_{CH} can be obtained from this doublet. In addition, from cross peak of the singlet, a value of long range J_{CH} can not be estimated, because long range J_{CH} of these cross peaks are less than two or three Hz.

The proton spectral data of portmicin indicated a gauche relationship between 3-H and 4-H ($J_{3,4}$=1.5Hz), but no information could be obtained with regard to the stereochemical relation between 4-H and C2 and 3-O-Me. The large coupling constant between 4-H and C2, which was determined to be $^3J_{CH}$=5.37 Hz based on the observed value (25 x J_{CH}=134.27 Hz), clearly established that 4-H and C2 are in an anti relationship. In addition, $^2J_{CH}$=6.6 Hz observed with 4-H to C3 indicated the gauche relationship between 4-H and 3-O-Me. As a result, stereochemistry of anti or gauche of the side-chain is decided easily.

Cross peak analysis of the methine proton connected to a methyl group with low sensitivity are generally difficult in the J-resolved HMBC spectra. In the Selective COSY-J-resolved-HMBC spectrum, analysis becomes easy only with methine signals being observed. Effective observation of signals with low intensity is important for J-resolved HMBC spectral analysis. The Selective COSY-J resolved-HMBC method is a method of choice for solving this problem.

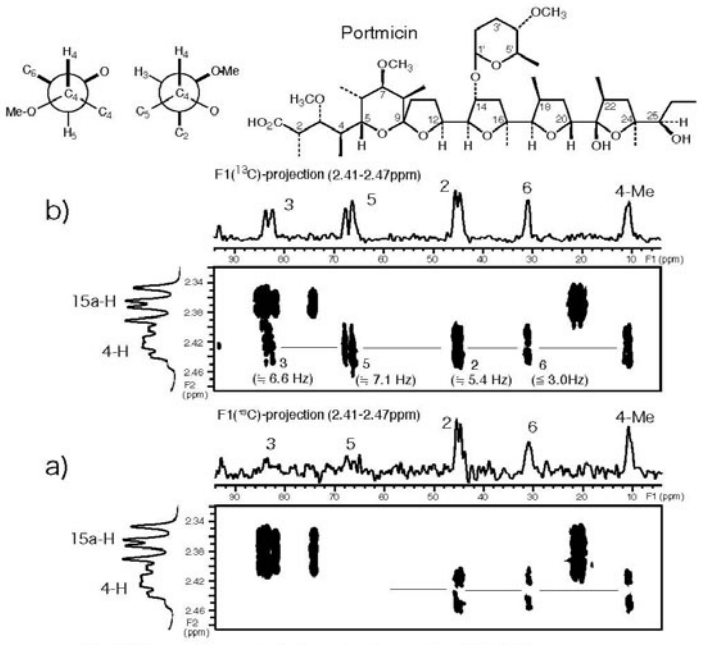

Fig.2 Portmicin a). Selective J-resolved HMBC
b).Selective COSY-J-resolved-HMBC-1
F_1 x F_2 = 14000 x 2500 Hz point = 256 x 2048
scaling factor(n) = 25 nt_1 max = 457 msec scans = 64

1). K. Furihata and H. Seto: *Tetrahedron.* 40 (1999) 6271-6275

2). K. Furihata, M. Tashiro and H. Seto: *Magn. Reson. Chem.* 47 (2009) 814–818

P-074
Y

Conformational analysis of poly(lactic acid) model compounds and the origin of the NMR chemical shift distribution due to the stereoregularity

Koto Suganuma[1,2], Ken Horiuchi[2], Hironori Matsuda[2], Akihiro Aoki[1], H.N.Cheng[3] and Tetsuo Asakura[1]

[1]Department of Biotechnology, Tokyo University of Agriculture and Technology,
[2]Material Analysis Research Laboratories, Teijin Ltd. and
[3]Agricultural Research Service, United States Department of Agriculture.

ABSTRACT

In order to understand the origin of the tacticity splitting in the NMR spectrum of poly(lactic acid), monomer model compound and dimer model compounds (both isotactic and syndiotactic) were synthesized and their ^{1}H and ^{13}C NMR chemical shifts observed. Two energetically stable conformations were obtained from Ramachandran map calculated as a function of the internal rotation angles for the monomer model using Gaussian 09 quantum chemical calculations. Four preferred conformations were selected for each isotactic and syndiotactic dimer model, and the conformations were again optimized. The ^{1}H and ^{13}C chemical shifts for isotactic and syndiotactic dimer model compounds were calculated by averaging the occurrence probabilities obtained from the optimized conformational energies and the calculated chemical shift of each conformation. Good agreement between observed and calculated chemical shifts was obtained for the relative chemical shifts of isotactic and syndiotactic ^{1}H and ^{13}C NMR peaks of the dimer model compounds. The observed tacticity splitting of poly(lactic acid) at the diad level was rationalized on the basis of these chemical shift calculations.

INTRODUCTION

Physical properties of poly (lactic acid) (PLA) are largely influenced by the stereoregularity and the distribution.[1] NMR is regarded as the best method to study polymer stereoregularity and therefore many NMR studies have been reported about the stereosequence distribution of PLA.[2,3]

In this work, we could clarify the origin of the tacticity splitting in the ^{1}H and ^{13}C NMR spectra of PLA using dimer model compounds and quantum chemical calculations. This is the first trial to understand the chemical shifts on the basis of the time-averaged conformations appeared in the solution.[4]

EXPERIMENT AND CALCULATION

The monomer model compound and the dimer model of PLA were synthesized. The ^{1}H and ^{13}C NMR data were obtained on a JEOL α-600 spectrometer operating at 600 and 150 MHz at room temperature. Deuterated chloroform was used as the solvent. The conformational energy calculations of model compound of PLA were carried out with Gaussian 09 software at TZVP base set. The magnetic shielding tensor was calculated quantum-chemically according to the GIAO method for ^{1}H and ^{13}C nuclei of the two preferred conformations of the model compound of PLA.

RESULTS AND DISCUSSION

(1) Ramachandran map and chemical shift calculation of monomer model compound

The conformational energies of monomer model compound,**1**, were calculated with Gaussian 09

as a function of the internal rotation angles, Φ and Ψ, and plotted as shown in Figure 1. According to our calculations, there are two energetically stable states at (Φ,Ψ) values of (-66°, 155°) and (-82°, 7°).

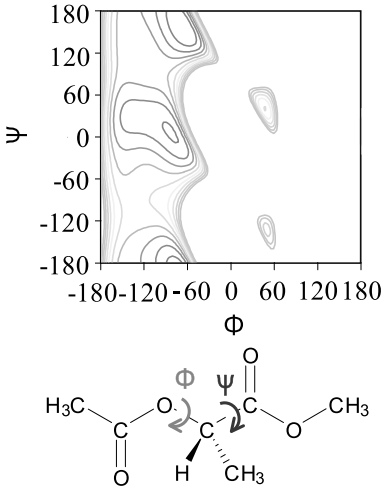

Figure 1. Ramachandran map of the conformational energies as a function of the internal rotation angles, Φ and Ψ for monomer model compound of PLA (**1**).

(2) Conformational energy calculations of the dimer model compound

The conformational energies of the four conformations for each isotactic and syndiotactic dimer model compound were calculated by the quantum chemical method. The combinations of energetically stable states of two preferred conformations selected from monomer model (**1**) were the initial four conformations of the dimer model and the each conformation was optimized. The energy difference (ΔE, in kJ/mol) and probability (%) of each conformation are listed in Table 1 together with the calculated ^{1}H and ^{13}C chemical shifts (ppm). As summarized in Table 1, the energetically most stable structure in isotactic dimer model compound is L1L1, and the probability is about 77%. Thus, the chemical shifts of the L1L1 conformation dominate the chemical shifts of isotactic dimer model compound. The conformational structure with the (Φ,Ψ) values of L1L1 looks like an α helix (10_3 helix), and the internal rotation angle of one carbonyl and the next carbonyl groups is 106°, which is similar to that of the α helix (108°). In contrast, the occurrence probability of the most stable conformation of L2D1 is only about 45%. Thus, in the case of syndiotactic dimer model, the contributions of the other three conformations become relatively large, contrary to the case of the isotactic dimer model compound.

Table 1. ^{1}H (upper) and ^{13}C (lower) chemical shifts (ppm) from TMS of the isotactic and syndiotactic dimer model compounds (**2**) together with the energy difference (ΔE) and probability (%) of each conformation.

type		isotactic						syndiotactic					
		Calcd.						Calcd.					
conformation		L1L1	L1L2	L2L1	L2L2	average	Obsd.	L1D1	L1D2	L2D1	L2D2	average	Obsd.
ΔE (kJ/mol)		0.00	3.71	8.03	9.04			3.11	0.96	0.00	3.45		
Probability (%)		77.3	17.5	3.1	2.1			13.0	30.6	45.1	11.3		
^{1}H	4	4.47	4.51	5.39	4.87	4.48	5.11	4.51	4.78	4.45	4.51	4.52	5.16
	7	4.56	4.60	4.46	4.56	4.57	5.17	4.05	4.54	4.48	4.55	4.51	5.15
	11	1.58	1.53	1.35	1.44	1.56	1.57	1.17	1.46	1.55	1.52	1.50	1.53
	12	1.46	1.48	1.42	1.43	1.46	1.53	1.14	1.45	1.38	1.41	1.39	1.51
^{13}C	4	66.01	65.50	64.33	65.11	65.96	68.30	59.61	64.76	66.92	66.42	66.22	68.44
	7	65.37	66.62	65.78	66.96	65.46	69.00	61.12	67.04	65.35	66.71	66.09	69.14
	11	16.65	16.57	16.42	17.65	16.63	16.68	15.78	16.55	17.14	17.23	17.05	16.77
	12	16.61	17.38	16.53	17.23	16.63	16.75	15.60	17.13	16.42	17.17	16.58	16.80
	2	182.87	182.71	181.45	182.11	182.84	170.33	172.31	182.46	182.96	182.82	182.80	170.14
	5	182.82	182.69	182.53	183.82	182.79	170.24	173.40	182.38	182.79	183.06	182.68	170.08
	8	183.55	183.67	182.83	183.34	183.56	170.65	173.50	183.41	183.11	183.65	183.28	170.44

(3) ^{1}H and ^{13}C chemical shift calculations of dimer model and comparison between the calculated and observed chemical shifts

The ^{1}H and ^{13}C chemical shifts were calculated with the quantum chemical method for all ^{1}H and

^{13}C nuclei of the four conformations for each isotactic and syndiotactic the dimer model compound. In each model compound, the relative occurrence probabilities of the preferred conformations were first calculated by Boltzmann distribution on the basis of the difference in the conformational energy. Since the chemical shifts were calculated for each conformation quantum-chemically, the chemical shift of each configuration could be obtained by taking into account both the relative occurrence probability and the chemical shifts of each conformation. The observed ^{1}H and ^{13}C NMR chemical shifts of the dimer model (**2**) were obtained in deuterated chloroform. The calculated ^{1}H and ^{13}C chemical shifts are compared graphically with the observed ^{1}H and ^{13}C chemical shifts (Figures 2) as stick spectra.

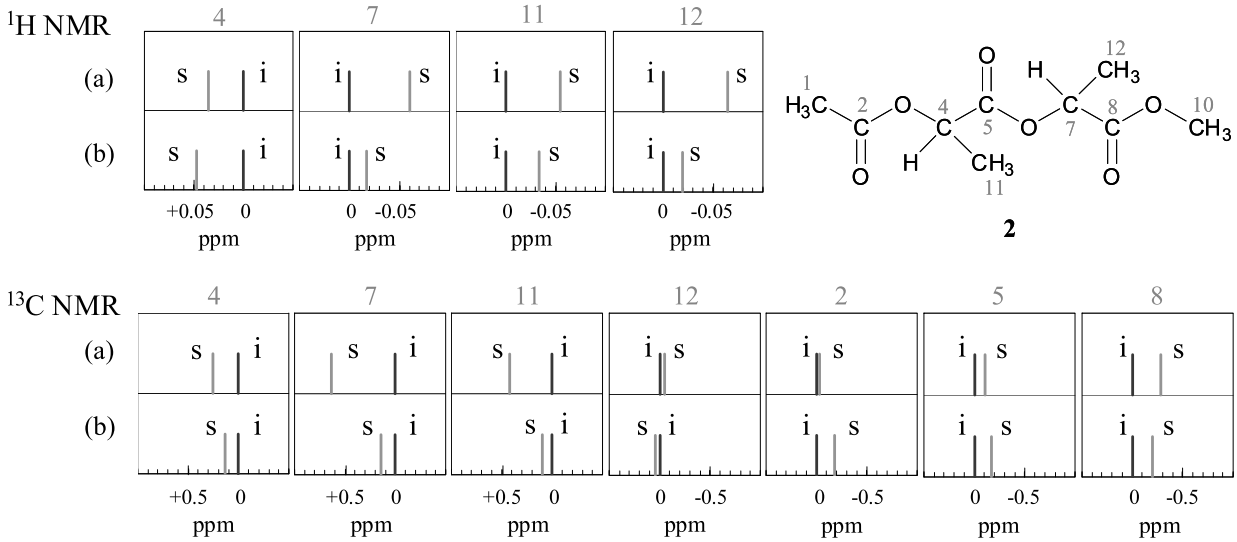

Figure 2. Comparison of the calculated and the observed ^{1}H and ^{13}C chemical shifts (in ppm) of dimer model compound (**2**) of PLA shown as stick spectra. (a) Calculated chemical shifts and (b) Observed chemical shifts. The chemical shifts are shown relative to the isotactic chemical shift. The blue stick corresponds to isotactic and the pink one syndiotactic.

As shown in Figure 2, good agreement between observed and calculated chemical shifts was obtained for the relative chemical shifts of isotactic and syndiotactic ^{1}H and ^{13}C NMR peaks of the dimer model compounds. And chemical shift calculations for isotactic and syndiotactic diad model (**2**) of PLA coupled with the conformational energy calculations can be used to predict time-averaged local conformation and tacticity splitting in this PLA dimer. The chemical shift is a good indicator that reflects the local conformations in solution.

(4) Analysis of PLA stereoregularity at the diad level on the basis of the chemical shift calculations of the diad model compounds

^{1}H and ^{13}C peaks of the CH group of PLA were assigned at the tetrad level. When the previous assignments of the tetrads are reduced to the diad level, an interesting trend can be seen. In the ^{1}H spectrum, the isotactic diad-centered tetrad peaks tend to resonate at lower field and the chemical shift range is relatively large compared with the syndiotactic diad-centered tetrad peaks. Contrary to the ^{1}H NMR case, in the ^{13}C NMR spectrum the syndiotactic diad-centered tetrad peaks resonate at lower field and the chemical shift range is relatively large compared with the isotactic diad-centered tetrad peaks. These trends are summarized in Figure 3, together with the calculated

and observed CH chemical shifts of the dimer model compounds mentioned above.

The positions of the calculated and the observed chemical shifts are shown relative to the isotactic peak. As noted above, the calculated syndiotactic H-7 appears upfield relative to the isotactic peak, but the opposite trend is found for H-4 in the dimer model compound. In PLA, the stereoregularity of the CH proton was reported to be more sensitive to the lactic acid units attached to the end with the hydroxyl group ("O-terminus")[3]. This corresponds to position 7 in the dimer model compound. Thus, the observed ^{1}H chemical shift of PLA should be compared with the calculated chemical shift of H-7, rather than H-4. For the calculated ^{13}C peaks, C-4 and C-7, the syndiotactic peaks appear downfield relative to the isotactic peaks in the dimer model compound. In PLA, the CH carbon was reported to be more sensitive to the lactic acid unit attached to the end with the carboxylic group ("C-terminus")[3], which corresponds to peak C-4 in the dimer model compound. Thus, the diad level splitting of ^{1}H and ^{13}C NMR spectra of the CH group of PLA can be satisfactorily interpreted by the chemical shift calculation performed here.

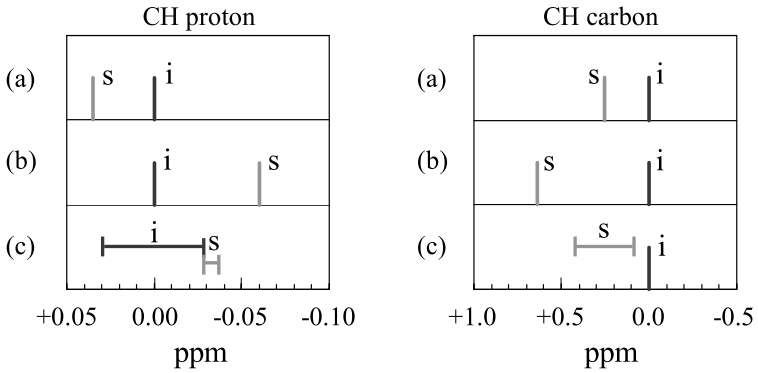

Figure 3. The calculated ^{1}H (left : (a)H-4, (b)H-7) and ^{13}C (right : (a)C-4, (b)C-7) chemical shifts (in ppm) of dimer model compound (**2**) of PLA. The observed ^{1}H (left: (c)) and ^{13}C (right: (c)) diad chemical shifts of PLA. All chemical shifts are shown relative to the isotactic chemical shift. The blue stick corresponds to isotactic and the pink syndiotactic.

The agreement between observed and calculated shifts in PLA means that the time-averaged local conformations predicted in this work are applicable to PLA in solution, and the origin of tacticity splitting in PLA is due to both time-averaged conformations and the chemical shifts of the conformations. At present, it is still unclear why the width of the tacticity splitting of the CH group in PLA is different for ^{1}H and ^{13}C. Further chemical shift calculation at the tetrad level of PLA by taking into account the time-averaged conformations for longer model compounds will hopefully provide more information in the future.

ACKNOWLEDGEMENT

The authors would like to thank Mr. Masato Komiyama at Teijin Pharma Ltd. for his support on the synthesis of the model compounds and Dr. Masao Hirasaka at Teijin Ltd. for his support on discussion.

REFERENCES

(1) Fukushima, K.; Kimura, Y. *Macromol. Symp.*, **2005**, *224*, 133-143.

(2) Bero, M.; Kasperczyk, J.; Jedlinski, Z. J. *Makromol. Chem.* **1990**, *191,* 2287-2296.

(3) Zell, M. T.; Padden, B. E.; Paterick, A. J.; Thakur, K.A.M.; Kean, R. T.; Hillmyer, M. A.; Munson, E. J. *Macromolecules* **2002**, 35, 7700-7707.

(4) Suganuma, K.; Horiuchi, K.; Matsuda, H.; Cheng, H.N.; Aoki, A.; Asakura, T. *Macromolecules* submitted.

Poly(lactic acid) model compound, Conformational analysis, Stereoregularity, Quantum chemical calculation

P-075

Y

Application of paramagnetic NMR to analyses of conformations and dynamics of oligosaccharides

Sayoko Yamamoto[1,2], Takumi Yamaguchi[2,3], Ying Zhang[2,3], Máté Erdélyi[4], Christian Griesinger[5] and Koichi Kato[1,2,3]
[1]Graduate School of Pharmaceutical Sciences, Nagoya City University
[2]National Institutes of Natural Sciences
[3]SOKENDAI
[4]Department of Chemistry, University of Gothenburg
[5]Department for NMR-Based Structural Biology, Max Planck Institute for Biophysical Chemistry

It is estimated that more than half of all proteins in nature are post-translationally modified with varying oligosaccharides. The oligosaccharides are critically involved in biomolecular recognition events mediating cell-cell communication and viral infections. In spite of their biological importance, there are still fewer reports describing 3D structures of the oligosaccharides in solution in comparison with those of proteins and nucleic acids. Although NMR spectroscopy offers powerful tools for structural analyses of biomolecules, the applicability of the widely used approach, i.e. NOE-based structural determination, is limited by insufficiency of the distance restraint information given the low proton densitiy in carbohydrates and the exceedingly low number of proton-proton NOEs that restrain interglycosidic linkages. In addition, quantitative interpretation of the NMR data of oligosaccharides associated with their dynamic properties also remains a challenging task. Hence, development of novel NMR methods is highly desirable for characterization of the glycan structures and investigation on their conformational flexibilities.

Here we propose paramagnetic-tagging method as a tool for NMR analyses of 3D structures of the oligosaccharides. Paramagnetic effects such as pseudocontact shifts (PCSs) induced by paramagnetic lanthanide ions with an anisotropic magnetic susceptibility tensor ($\Delta\chi$ tensor) offer long-distance information on conformations and dynamics of biomolecules. We focused on the lanthanide-induced PCS of the CH groups of glycan to extract unique information on its glycosidic linkage conformation. An EDTA derivative was designed as the tag to chelate a lanthanide ion (see Scheme 1). A rigid phenylene spacer was inserted to suppress unfavorable relaxation enhancement of the carbohydrate resonances originating from the nuclei spatially proximal to the coordinated paramagnetic metal ion. The rigidity of the tag as well as the stability of the lanthanide complex are crucial factors for unambiguous interpretation of the PCS data.

To develop a general method, we focused on *N*,*N*'-diacetylchitobiose, the common core structure shared among all *N*-linked oligosaccharides, which form a major class of the glycoprotein glycans. The lanthanide tag was covalently attached to the reducing terminals of this disaccharide through an amide linkage that mimics the *N*-glycans (Scheme 1). The addition of up to one molar equivalent of

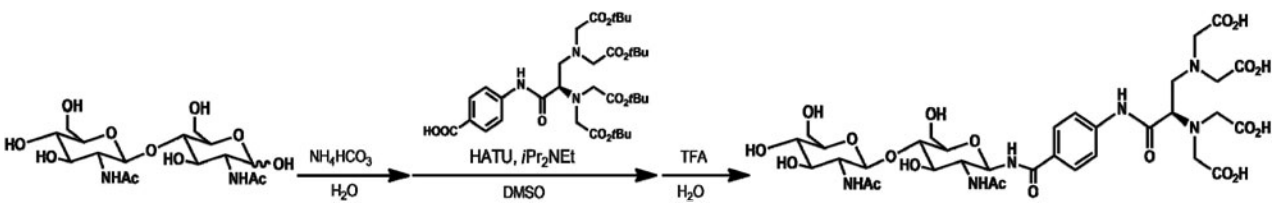

Scheme 1. Introduction of the lanthanide-chelating unit to *N*,*N*'-diacetylchitobiose.

the paramagnetic lanthanide ion such as Tm^{3+} and Ho^{3+} generated a new set of peaks originating from tagged sugar with concomitant disappearance of the original peaks. By ^{1}H-^{13}C HSQC experiments, the PCSs were measured as the differences of ^{1}H and ^{13}C chemical shifts compared with the compound chelated to the diamagnetic La^{3+} (Figure 1a). The observed PCSs were largest (1.1 ppm) for C1, the anomeric carbon located at the reducing terminus, and smaller for the more distal atoms.

For conformational analysis of *N*,*N*'-diacetylchitobiose, molecular dynamics (MD) simulation in explicit water was performed employing AMBER 11 software package with GLYCAM_06 force filed. This potentially enables adequate conformational sampling of glycosidic linkage, which has restricted numbers of energetically accessible conformations and relatively small differences in their free energies. The result of MD simulation indicated the conformational rigidity of the glycosidic linkage of this disaccharide. Accordingly, the structural model of lanthanide- tagged disaccharide was built with the torsional angles defined by H1-C1-O4'-C4' and C1-O4'-C4'-H4' of 63° and 18°, respectively (Figure 1b). The axial and rhombic components of the $\Delta\chi$ tensor were determined for this model by using the experimentally obtained PCSs. The back-calculated PCSs are in excellent agreement with the experimental data (Figure 1c). This indicates that the common innermost part of the *N*-linked oligosaccharides exhibit rigid conformations, which is little affected by the attachment of a tag. Hence, this method is applicable for a variety of *N*-linked glycans including those with more flexible conformations.

On the basis of these results, we conclude that the paramagnetic NMR approach in conjunction with MD simulation can provide valuable information on conformations and dynamics of oligosaccharides. It opens the door to conformational studies various carbohydrate chains of biological interest.

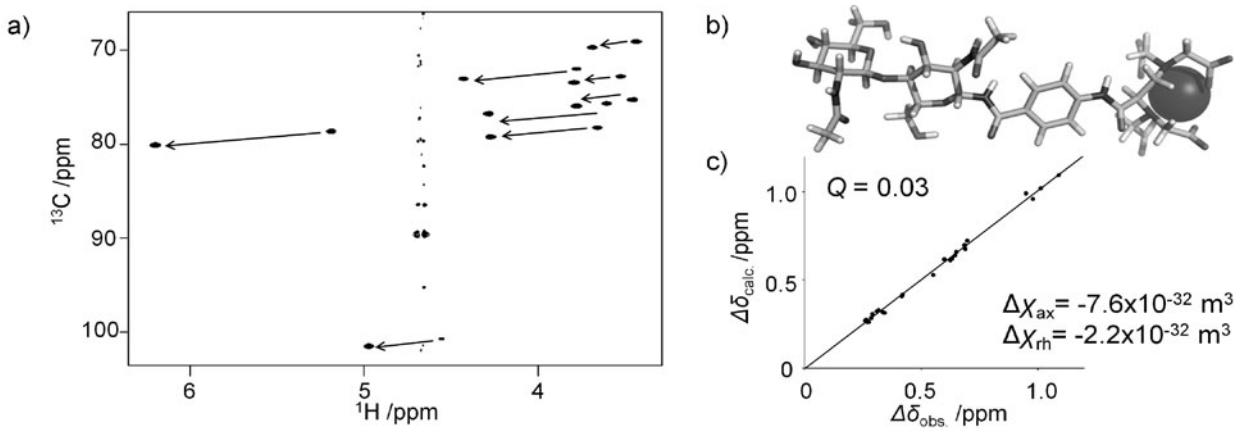

Figure 1. The analysis of PCS of the modified *N*,*N*'-diacetylchitobiose. a) ^{1}H-^{13}C HSQC spectra of tagged disaccharide complexed with Tm^{3+} and La^{3+}. The chemical shift perturbation of the CH groups is indicated by arrows. b) The structural model of tagged disaccharide. c) The axial and rhombic components of the $\Delta\chi$ tensor ($\Delta\chi_{ax}$, $\Delta\chi_{rh}$) and correlation plot between the observed and back-calculated PCSs.

Reference

[1] S. Yamamoto, T. Yamaguchi, M. Erdélyi, C. Griesinger and K. Kato
Chem. Eur. J., **17**, 9280-9282 (2011)

oligosaccharide, pseudocontact shift, lanthanide

P-076
Y

Degradation of liquid organic semiconductors analyzed by NMR

Junichi Yamamoto[1], Masashi Fukuchi[1], Tatsuya Fukushima[1], Shuzo Hirata[2], Heo Hyo Jung[2], Osamu Hirata[2,3], Yuki Shibano[3], Chihaya Adachi[2] and Hironori Kaji[1]
Institute for Chemical Research, Kyoto Univ. [1], OPERA, Kyusyu Univ. [2], Nissan Chemical Industries, LTD[3]

Liquid organic light-emitting diodes (liquid OLEDs) are recently-developed OLEDs consisting only of liquid organic semiconductors in the active layer. The liquid OLEDs have unique characteristics and have a potential to solve present problems of organic devices. In this study, we have investigated material degradation in liquid OLEDs by solution NMR. The NMR spectra clearly indicate that the dimerization of liquid organic semiconductor we used occurs in the liquid OLEDs, which is considered to be related to the device degradation.

[Introduction]

Recently, we have developed liquid OLEDs [1,2]. This novel OLED is expected to allow the realization of truly flexible displays, which will solve problems of cracks and shortage of OLEDs. However, the fundamental characteristics are at a primitive stage and the device lifetime is very short at present. To overcome this problem, it is important to reveal the degradation mechanism, which will provide guidelines for material designs with long lifetimes. In this study, we have investigated material degradation in liquid OLEDs by solution NMR.

[Experimental]

Fig. 1 shows the chemical structures of compounds used in this study. TEGCz and tetrabutylammonium hexafluorophoshate (TBAHFP) were used as the liquid host and electrolyte, respectively, and TBAHFP was doped into the TEGCz layer. Liquid OLEDs were composed of ITO/0.25 wt% TBAHFP, TEGCz (10 μm)/ITO. The material degradation was investigated for the devices driven at 1 mA for 11, 30, and 50 s.

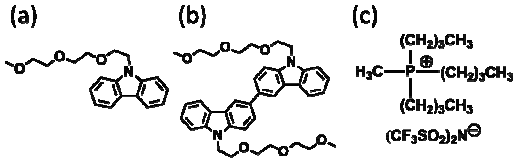

Fig. 1. Chemical structures of (a) TEGCz, (b) $(TEGCz)_2$, and (c) TBAHFP.

Two different solution NMR experiments were performed to reveal material degradation in liquid OLEDs. First, we carried out ^{1}H NMR experiments of TEGCz with 0.25 wt% TBAHFP after the degradation for 11, 30, 50 s. ^{1}H NMR experiments of TEGCz and $(TEGCz)_2$ with 0.25wt% TBAHFP before degradation were also carried out for comparison. Second, diffusion-ordered NMR spectroscopy (DOSY) measurements were carried out to separate organic materials in the devices after degradation. The DOSY measurements also provide the estimate of diffusion

organic light-emitting diodes, liquid organic semiconductors, degradation, dimerization, DOSY

coefficients of these materials. All experiments were carried out in dichloromethane-d_2 and on a Bruker AVANCE Ⅲ 600MHz US Plus spectrometer with a double resonance 1.7 mm probe.

[Result and discussion]

Fig. 2 shows ^{1}H NMR spectra of TEGCz with 0.25 wt% TBAHFP (a) before degradation and (b) after degradation for 50 s. Here, we only show a region from 7.7 to 8.5 ppm. A large peak at 8.08 ppm is assigned to ^{1}H in TEGCz, and * marks in the figure represent carbon satellites for the peak of TEGCz at 8.08 ppm. The peaks at 8.43, 8.18, and 7.86 ppm, which were not observed in Fig. 2(a) (in the device before degradation), were clearly found in Fig. 2(b) (in the device after degradation). To clarify the origin of these peaks, we searched and measured several possible molecules, which provide these peaks. As a result, we found that dimerization reactions occur in the devices. Fig. 2(c) shows a ^{1}H NMR spectrum of $(TEGCz)_2$ with 0.25 wt% TBAHFP. The peaks in Fig. 2(c) agree well with those in the device after degradation in Fig. 2(b) at 8.43, 8.18, 7.86 ppm. All the peaks of $(TEGCz)_2$ were found in the devices after degradation not only in the chemical shift region in Fig. 2 but also in all the chemical shift regions. The intensities of these peaks increase with increasing the device driving time, 11, 30, 50 s. Therefore, it is found that $(TEGCz)_2$ is produced as a result of driving the devices.

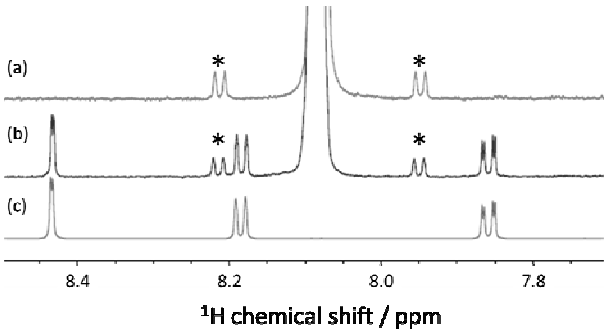

Fig. 2. ^{1}H NMR spectra of TEGCz with 0.25 wt% TBAHFP; (a) before and (b) after degradation for 50 s. ^{1}H NMR spectrum of $(TEGCz)_2$ with 0.25 wt% TBAHFP before degradation is also shown in (c) for comparison.

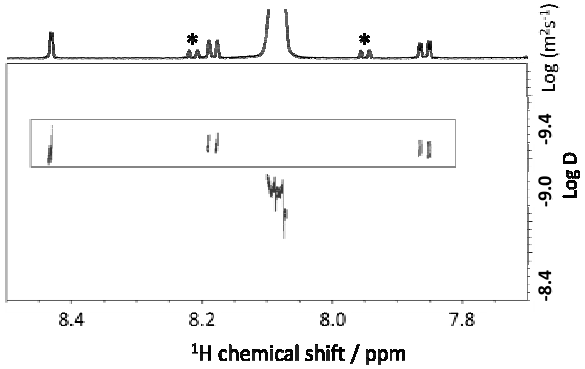

Fig. 3. A DOSY contour plot of TEGCz with 0.25 wt% TBAHFP after degradation for 50 s.

We carried out DOSY to further explore the dimerization of TEGCz. Fig. 3 shows a DOSY contour plot of TEGCz with 0.25 wt% TBAHFP after degradation for 50 s. From Fig. 3, it is found that a diffusion coefficient of a degraded molecule is smaller than that of TEGCz. This result shows that the degraded molecule is larger than TEGCz. From the above NMR experiments, we found that the dimerization of TEGCz occurred in the liquid OLEDs by driving the devices.

[Reference]

[1] D. Xu and C. Adachi, *Appl. Phys. Lett.*, **95**, 053304 (2009).

[2] S. Hirata, K. Kubota, H. H. Jung, O. Hirata, K. Goushi, M. Yahiro, and C. Adachi, *Adv. Mater.*, **23**, 889 (2011).

[Acknowledgment]

This research is granted by the Japan Society for the Promotion of Science (JSPS) through the “Funding Program for World-Leading Innovative R&D on Science and Technology (FIRST Program),” initiated by the Council for Science and Technology Policy (CSTP).

P-077 Stereochemical analysis of functionalized bispidinones by NMR techniques

Paramasivam Parthiban and Dong Ho Park

Department of Biomedicinal Chemistry, Inje University, Gimhae, Korea

ABSTRACT

Bispidinone is the important class of nitrogen heterocycle owing to their presence in the naturally occurring lupin alkaloids and diverse biological actions. In fact, bispidinone is a scaffolds of the biologically significant piperidone, and hence, we planned to synthesize a series of 2,4,6-8-tetraaryl-3,7-diazabicyclo[3.3.1]nonan-9-ones by adopting the modified Mannich condensation of acetone, ammonium acetate and aldehydes in 1:2:4 M ratio. The targeted product is an outcome of four successive Mannich condensations. In order to improve the yield and selectivity, we have employed PPA.SiO_2 as well as BF_3.SiO_2 as heterogeneous catalysts and as a result, all the bispidinones were achieved as a single isomer with good yields. Generally, these types of bicycles may adopt either chair-chair or chair-boat or boat-boat conformations as depicted in Figure 1.

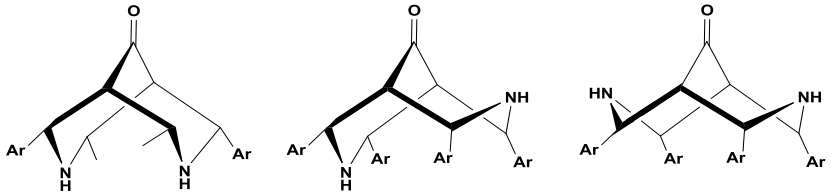

Fig.1: Possible chair-chair, chair-boat and boat-boat conformations of the bicycle.

The conformation of the bicycle and configuration of the substituents will vary with the nature and position of the substituents on the heterocycle. Similarly, biological actions also depend on the nature/position of the substituents as well as stereochemistry of the molecule. Hence, it is immense helpful to establish the stereochemistry in the sense of biological perception.

In order to find the impact on the stereochemistry of the bispidinone bicycle and for their pharmacological utility, we have synthesized a series of fourty 2,4,6-8-tetraaryl-3,7 -diazabicyclo[3.3.1]nonan-9-ones with various substituents such as halo/alkyl/alkoxy/ hodroxy/phenoxy/benzyloxy/allyloxy/thioalkoxy/morpholine substituents alone at *ortho/meta/para* position or together on the various positions of the phenyl groups. To our surprise, all compounds exist in the chair-boat conformation, irrespective of the nature and/or position of the substituents on the phenyl. The phenyl groups in the chair form adopt an equatorial orientation as seen in Figure 2.

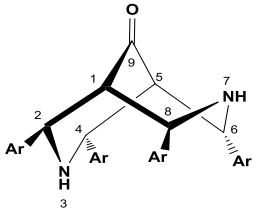

Fig.2: Chair-boat conformation of the target compounds with an equatorial disposition of the aryl groups in the chair part is unambiguously confirmed by their H,H-COSY and NOESY correlations.

It is very important to point out that, for the target molecules a number of stereomers are possible as witnessed by their stereogenic centers. However, all aldehydes specifically yielded the target molecules as shown in Figure 2. And one more vital factor is none of the products required even column purification. The proton and carbon chemical shits of the compounds were unambiguously carried out with the help of H,H-COSY/NOESY and HSQC/HMBC correlations, respectively, and a few cases, SEFT and DEPT were also utilized.

The NMR investigation clearly brings out the insight of the substituents effect versus position. Even though both the *ortho* and *meta* isomers exhibit the same stereochemistry as *para* isomer, the ^{1}H and ^{13}C chemical shifts of the *ortho* isomer are significantly away from the *meta* and *para* isomers, but the difference between *meta* and *para* isomers are negligible. And particularly in *ortho* isomers, both the ^{1}H and ^{13}C chemical shifts of benzylic (H-2/H-4/H-6/H-8) and bridge-head protons (H-1/H-5) and their attached carbons are significantly spaced out from their *meta* and *para* counterparts. The magnitude of impact depends on the electron withdrawing/donating nature and electronegativity magnitude of the substituents on the phenyl.

The deshielding of protons is reasonably associated by the interaction between the halogens and benzylic/bridge-head protons. Similarly in alkoxy substituted compounds, the non-bonded interaction exist between the above said ring protons and oxygen of the alkoxy substituents by the electronic effect of the alkoxy groups attached on the *ortho* position of the phenyl (Fig. 3). Of them, the interaction is strong with the benzylic protons than the bridge-head protons owing to their spatial proximity. In the above cases, the C-X or C-O bonds of the *ortho* substituents prefer to be *syn* to the benzylic protons to avoid the C-X/C-O and C-N dipole–dipole interactions.

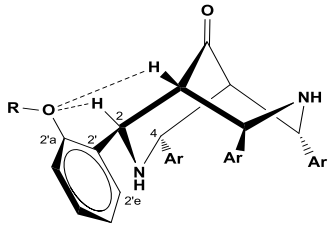

Fig.3: The interactions between the oxygen of the alkoxy substituents or halo substituents and the ring protons flatten the bonds between C-1 and C-2 as well as C-4 and C-5.

As a consequence of the above interactions, the *ortho* protons (H-2'e and H-4'e) of the chair conformation are more nearby to the axially oriented nitrogen lone pair. Thus it makes more favorable arrangement to interact with the *ortho* protons and deshielding them significantly. The interactions, one between substituents at *ortho* position and ring protons and another between *ortho* protons and nitrogen lone pair make an apparent restricted rotation of the phenyl rings. In order to clarify this, we have carried out dynamic ^{1}H NMR study on some representative compounds between the temperature range -55 to 55 ^{o}C (218-318 K) in $CDCl_3$. But the absence of significant broadenings and indicative coalescence suggest that the restricted rotation and energy barrier are not remarkable on these molecules.

P-078 High-Pressure Multinuclear NMR Analyses of Lewis Acid-Lewis Base Interactions between Boron Compounds and Uranyl β-Diketonato Complexes in Supercritical CO_2

Naomi Miyamoto, Takehiko Tsukahara, Yoshihiro Kachi, Masayuki Harada, and Yasuhisa Ikeda
Research Laboratory for Nuclear Reactors, Tokyo Institute of Technology

INTRODUCTION

Supercritical carbon dioxide ($scCO_2$) has attracted attention as a novel reaction medium for treating radioactive wastes contaminated with uranium, which are produced from various processes in the nuclear fuel cycle. In order to extract uranyl species efficiently from such radioactive wastes to $scCO_2$ phase, the solubility control of uranyl species into $scCO_2$ is one of the most important factors. Previously, we examined the solubility of various metal complexes in $scCO_2$ using UV-vis and NMR spectrometers, and found that uranyl complexes with oxo groups (U=O) have higher solubility than other metal complexes without oxo groups [1]. This suggests that the relatively high solubility of uranyl complexes in $scCO_2$ is due to the local Lewis Acid (LA)-Lewis Base (LB) interactions between CO_2 and uranyl oxygen (abbreviated as U=O). However, the existence of such interactions has not been proved sufficiently.

In this study, hence, in order to clarify whether the U=O can act as LB in $scCO_2$, we have examined ^{11}B-, ^{17}O-, and ^{19}F-NMR chemical shifts of samples prepared by dissolving LA compounds ($B(C_6F_5)_2OH$) and uranyl complexes in $scCO_2$ and organic solvents. As the uranyl complexes with and without the fluorinated ligands, $UO_2(dfh)_2DMSO$ and $UO_2(acac)_2DMSO$ were selected, respectively.

EXPERIMENTAL

$B(C_6F_5)_2OH$ was synthesized by the hydrolysis of tris(pentafluorophenyl)borane $B(C_6F_5)_3$[2]. The $UO_2(dfh)_2DMSO$ and $UO_2(acac)_2DMSO$ complexes were synthesized according to previous paper[3]. $B(C_6F_5)_3$ (Tokyo Chemical Industry Co., Ltd.), 1,1,1,2,2,6,6,7,7,7-decafluoro-3,5-heptanedione (Hdfh, Matrix Scientific), and 2,4-hepatanedione (Hacac, Kanto Chemical Co., Ltd.) were used without further purification. Dimethyl sulfoxide (DMSO), toluene (Kanto), and CO_2 gas (purity of 99.999%, TOMOE SHOKAI Co., Ltd.) were stored over molecular sieves 4A before use.

Details of NMR apparatus used in this study have been described elsewhere [4]. Briefly, after charging samples into the zirconia NMR sample tube, the sample tube was sealed with the stainless sample holder and o-ring in the glove box. NMR spectra of toluene solutions were measured at 25 $^\circ$C, and those of $scCO_2$ were measured under the conditions of 40 $^\circ$C and 10.0 - 25.0 MPa. The ^{11}B, ^{17}O, and ^{19}F-NMR chemical shifts were referenced to $BF_3 \cdot OEt_2$ (0 ppm), mixture of D_2O and 1,4-dioxane (0 ppm), and fluorobenzene (-113 ppm), respectively.

RESULTS AND DISCUSSIONS

^{11}B-NMR spectra in toluene and $scCO_2$

The ^{11}B-NMR spectra of toluene solutions dissolving $B(C_6F_5)_2OH$ and $UO_2(dfh)_2DMSO$ or $UO_2(acac)_2DMSO$ were measured. The results are shown in Fig.1. The ^{11}B-NMR peak of toluene solution dissolving $B(C_6F_5)_2OH$ was observed at 40 ppm. This is consistent with previous paper[5]. Their chemical shifts were almost constant regardless of changes of the concentrations of $B(C_6F_5)_2OH$ and the addition of $UO_2(dfh)_2DMSO$. These results indicate that there are no apparent interactions between U=O of $UO_2(dfh)_2DMSO$ and $B(C_6F_5)_2OH$ in toluene. On the other hand, in the toluene solution dissolving $UO_2(acac)_2DMSO$ and $B(C_6F_5)_2OH$, new ^{11}B-NMR peak(δ_{new}) was observed around 5 ppm with the peak assigned to $B(C_6F_5)_2OH$ at 40 ppm ($\delta_{initial}$). The δ_{new} is

characterized as the peak associated with the interactions between $UO_2(acac)_2DMSO$ and $B(C_6F_5)_2OH$, because the ^{11}B-NMR spectrum of $B(C_6F_5)_3$, which is similar LA compounds to $B(C_6F_5)_2OH$, is well known to be shifted toward high magnetic field by the coordination to U=O [5]. Moreover, the peak area ratios of δ_{new} to $\delta_{initial}$ were found to decrease with increasing concentration of $B(C_6F_5)_2OH$, i.e., from 1.1 for system of $[B(C_6F_5)_2OH] = 2.8 \times 10^{-3}$ M (M = mole dm^{-3}) to 0.3 for that of $[B(C_6F_5)_2OH] = 7.5 \times 10^{-3}$ M. The behavior of δ_{new} suggest that U=O of $UO_2(acac)_2DMSO$ directly interact with $B(C_6F_5)_2OH$ in toluene and that two molar equivalent of $B(C_6F_5)_2OH$ interacts with one $UO_2(acac)_2DMSO$.

In the same way, we measured the ^{11}B-NMR spectra of $B(C_6F_5)_2OH$ and $UO_2(dfh)_2DMSO$ or $UO_2(acac)_2DMSO$ dissolved in $scCO_2$, and found that their ^{11}B-NMR chemical shifts were almost similar to those of toluene. The results indicate that the Lewis basicity of U=O are induced in $UO_2(acac)_2DMSO$, but not in $UO_2(dfh)_2DMSO$.

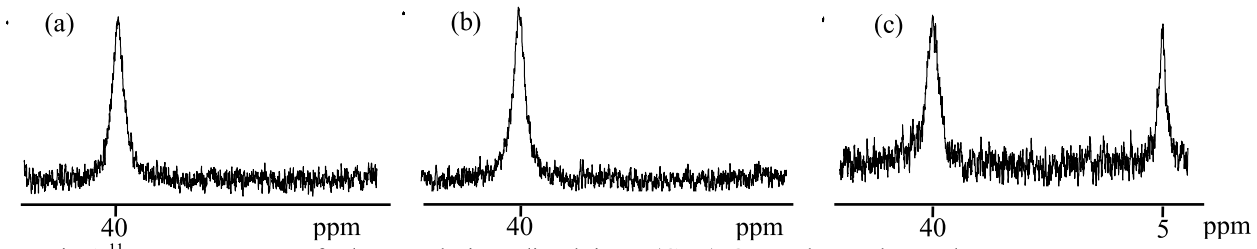

Fig.1 ^{11}B-NMR spectra of toluene solutions dissolving $B(C_6F_5)_2OH$ and uranyl complex.
(a) $[B(C_6F_5)_2OH] = 5.0 \times 10^{-3}$ M, (b) $[UO_2(dfh)_2DMSO] = 1.0 \times 10^{-3}$ M, $[B(C_6F_5)_2OH] = 5.0 \times 10^{-3}$ M,
(c) $[UO_2(acac)_2DMSO] = 1.0 \times 10^{-3}$ M, $[B(C_6F_5)_2OH] = 5.0 \times 10^{-3}$ M

^{17}O-NMR chemical shift in toluene

If the $B(C_6F_5)_2OH$ interacts directly with U=O of $UO_2(acac)_2DMSO$, the ^{17}O-NMR chemical shifts are expected to be also affected by addition of $B(C_6F_5)_2OH$. Therefore, we measured ^{17}O-NMR spectra of $B(C_6F_5)_2OH$ and $UO_2(dfh)_2DMSO$ or $UO_2(acac)_2DMSO$ dissolved in toluene. In spite of the addition of $B(C_6F_5)_2OH$ the ^{17}O-NMR chemical shifts of $UO_2(dfh)_2DMSO$ dissolved in toluene were observed at 1160 ppm. On the other hand, the ^{17}O-NMR chemical shifts of $UO_2(acac)_2DMSO$ were shifted from 1155 ppm to 1144 ppm by addition of $B(C_6F_5)_2OH$. Such higher field shift verify the existence of LA-LB interaction between U=O of $UO_2(acac)_2DMSO$ and $B(C_6F_5)_2OH$.

CONCLUSION

In this study, we have observed ^{11}B-NMR spectra of $B(C_6F_5)_2OH$ and uranyl complexes dissolved in toluene and $scCO_2$ and ^{17}O-NMR spectra of these compounds dissolved in toluene. As a result, it is suggested that the LA-LB interactions between $B(C_6F_5)_2OH$ and $UO_2(acac)_2DMSO$ exist in toluene and $scCO_2$. In addition, it is proposed that the magnitude of LA-LB interactions is reduced with increasing fluorine atoms of uranyl complexes.

REFERENCE

[1] T. Tsukahara *et al.*, *J. Supercrit. Fluids.*, **39**, 6-12 (2006)
[2] I. Ikeno *et al.*, Patent WO 02/44185, (2000)
[3] K. Mizuguchi *et al.*, *J. Alloy. Compd.*, **271**, 163-167 (1998)
[4] T. Tsukahara *et al.*, *J. Phys. Chem. B*, **112**, 16445-16454 (2008)
[5] M.J. Sarsfield *et al.*, *J. Am. Chem. Soc.*, **126**, 1036 -1037(2004)

Supercritical CO_2, ^{11}B- and ^{17}O-NMR spectra, Uranyl β-diketonato complexes

P-079 Determination of dynamic structure and orientation of alamethicin bound to the acidic lipid bilayers by solid-state NMR spectroscopy

Jun Wang[1], Atsushi Tsutsumi[1], Kiyonobu Yokota[2], Izuru Kawamula[1] and Akira Naito[1]
[1]Graduate School of Engineering, Yokohama National University, Yokohama.
[2]Computational Biology Research Center, National Institute of Advanced Industrial Science and Technology, Tokyo.

【Abstract】

Dynamic structure and orientation of alamethicin in the acidic lipid bilayers were determined by using solid-state NMR to observe fully anisotropic, partially anisotropic ($\Delta\delta$) and isotropic ^{13}C chemical shifts in the carbonyl carbon of the peptide under the CP-MAS (2kHz), DD-static and DD-MAS (4kHz) experiments, respectively. Moreover, chemical shift oscillations were analyzed by considering the rotational motion of the helix about the bilayer normal with the tilt angle ζ of the helical axis and the phase angle γ of the peptide plane. The ζ and γ were determined by inspecting RMSD plots between calculated ($\Delta\delta_{cal}$) and experimentally obtained values ($\Delta\delta_{obs}$).

【Introduction】

Alamethicin is an antimicrobial peptide consisting of 20 residues, produced by the fungus *Trichoderma viride*. In cell membranes, an oligomerization of a few alamethicin molecules forms a voltage-dependent ion channel. When potential is applied, a helical bundle is inserted into the membrane to open the ion channel. The structure of alamethicin bound to neutral bilayers has been determined by solid-state NMR in our previous study[1]. It turned out that alamenthicin or its oligomerization adopts a bent pseudo-transmembrane orientation in neutral bilayers, with tilt angles of 17° for the N-terminal α-helix and 32° for the C-terminal 3_{10}-helix. In this study, we will show the structure and orientation of alamethicin in the acidic membrane as a mimic of bacterial membrane.

【Experimental】

[1-^{13}C]Ala^{6}, Val^{9}, Leu^{12}, Aib^{13}, Aib^{16}-labeled alamethicin samples were synthesized by Fmoc-chemistry and solid phase method and incorporated into the acidic lipid bilayers. N-terminal acetylation and deprotection were performed. Then, the C-terminal was esterificated and the product was purified by HPLC. All samples were then incorporated into acidic lipid bilayers (the morlar ration of peptide : lipid is 1 : 10 in Tris buffer) following the procedure in our previous work[2].

Keyword: Solid-state NMR, Alamethicin, Chemical shift oscillation

Finally, we used solid state NMR to observe anisotropic chemical shift values in the carbonyl carbon of the peptide and determined the structure and orientation of alamethicin in the acidic lipid bilayers. DD-MAS (4kHz) and DD-static experiments with the fully hydrated sample, and CP-MAS (2kHz) experiments with the lyophilized sample were performed by using CMX-400 Infirmity Solid State NMR Spectrometer.

【Results and Discussion】

We observed isotropic, partially anisotropic ($\Delta\delta$) and fully anisotropic (δ_{11}, δ_{22}, δ_{33}) ^{13}C chemical shifts in the carbonyl carbon of the peptide under the DD-MAS, DD-static and CP-MAS experiments, respectively. Isotropic ^{13}C chemical shifts obtained from DD-MAS experiments show that alamethicin takes a helical structure. From the DD-static experiments, all resulting powder patterns clearly show the axially symmetric shapes, indicating that alamethicin molecules rotate about a unique axis. Namely, the rotation axis of alamethicin is known to be parallel to the bilayer normal[1]. $\Delta\delta_{obs}$ values were determined by inspecting the powder patterns. Moreover, the chemical shift oscillation behavior of $\Delta\delta$ against residue numbers was analyzed by considering the rotational motion of the helix about the bilayer normal with the tilt angle ζ and the phase angle γ of the peptide plane. The ζ and γ were determined by inspecting RMSD plots between calculated ($\Delta\delta_{cal}$) and experimentally obtained values ($\Delta\delta_{obs}$) for the N- and C-terminal helices, respectively.

The above results indicate that the alamethicin in the acidic lipid bilayers may adopt transmembrane bending helix and the N-terminal (1~10 residues) and C-terminal (11~20 residues) regions form α-helical structures with the tilt angles of 17° and 31° to the bilayer normal, respectively (Fig.1). However, in the same bilayers the structure around Leu[12] and Aib[13] in the C-terminal was revealed to be a 3_{10}-helical structure with the tilt angle of 35° to the bilayer normal in the case where the RMSD value was analyzed using the $\Delta\delta_{obs}$ date of Leu[12] and Aib[13]. This structure is almost consistent with that of alamethicin in the DMPC neutral bilayers. In addition, if the chemical shift dates of the other labeled samples are measured, I could get the more detailed structure and the tilt angle

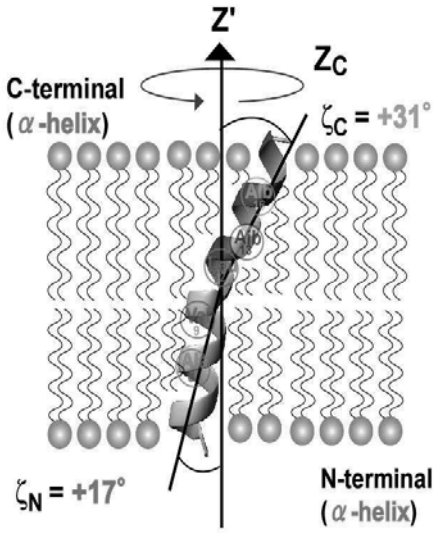

Fig.1 Alamethicin in the acidic lipid bilayers

1. A.Naito, Solid State Nuclear Magnetic Resonance, 36 (2009) 67-76.
2. S.Toraya, N.Javkhlantugs, D.Mishima, K.Nishima, K.Ueda, and A.Naito, Biophysical Journal, 99 (2010) 3282-3289.

P-080

Y

DNP with photoexcited triplet electrons in thin film

Kenichiro Tateishi[1], Makoto Negoro[1], Akinori Kagawa[1]
and Masahiro Kitagawa[1]
[1]Graduate School of Engineering Science, Osaka University

ABSTRACT

Improvement of the sensitivity with Dynamic Nuclear Polarization (DNP) opens new possibilities in the study on thin film, surface, and interface. With DNP using photoexcited triplet electrons of pentacene, nuclear spin polarization can be increased to on the order of 0.1 even at room temperature with simple experimental equipment. In this work, the proton polarization of 0.074 was obtained in a thin film of 0.05 mol% pentacene doped p-terphenyl in 0.4 T at room temperature. The thin film was fabricated by "cell method" and its thickness is 2.4 μm.

The study on thin film, surface, and interface using NMR has been extensively investigated in recent years. In conventional NMR, it is difficult to obtain these signals because strong signals from bulk portions shroud them. Improvement of the sensitivity with Dynamic Nuclear Polarization (DNP) opens new possibilities not only in general NMR spectroscopy but also for these studies. Lesage *et al.* succeed in enhancing surface signals of silica with DNP using free radicals [1]. However expensive and complex equipment such as cryogenic technology or millimeter wave technology are required for these experiments. On the other hand, with DNP using photoexcited triplet electrons of pentacene (triplet-DNP), nuclear spin polarization can be increased to on the order of 0.1 even in low magnetic field at room temperature with simple experimental equipment [2]. For pentacene, the polarization of the triplet state is nearly 0.7 and is independent of static magnetic field and temperature. Furthermore owing to the finite lifetime of the triplet electron spins, the nuclear spins become free from disturbance by the electron paramagnetism during measurements.

We plan to investigate a small amount of samples deposited on a single crystal of pentacene doped p-terphenyl. Signals from an organic or biological sample of interest on the surface can be amplified by transferring hyperpolarized spin state through the organic-organic interface. By applying triplet-DNP, the state in pentacene molecule spreads to the surrounding host molecules via spin diffusion process. Since the diffusion constant is very small ($\sim 10^{-16}$ m^2/s) [3], the spin state may only transport a few μm per an hour. In order to make the deposited sample signal legible, it is desirable to use a small single crystal. In this work, we fabricated thin film of pentacene doped p-terphenyl by "cell method" [4] and the proton polarization was enhanced with triplet-DNP

Keyword : triplet-DNP, thin film, cell method

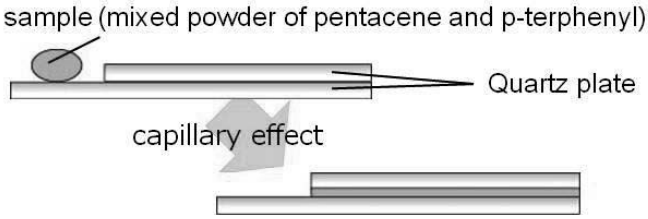

Fig. 1: Schematically illastrated cell method. Mixed powder of pentacene and p-terphenyl were inserted in a narrow gap of quartz cell by capillary effect, and thin crystal was grown from melt.

Single crystals of thin films were easily grown by Cell method. Mixed powder of pentacene and p-terphenyl were inserted in a narrow gap of quartz cell by capillary effect, and thin crystal was grown from melt (Fig. 1). Compared to sublimation method, much higher concentration of pentacene was attained. By adjusting the gap, the thin film of about 1 to 100μm thickness can be made. The thin film of 0.05 mol% pentacene doped p-terphenyl was grown by this method and its size was 2.4 μm × 0.7 mm^2.

Triplet-DNP experiments were carried out in 0.402 T (^{1}H: 17.188 MHz) at room temperature using home-made X-band system. Flashlamp pumped pulsed dye laser (Cynosure, LFDL-3) was used to excite pentacene efficiently. Using the sample, the proton polarization of 0.074 was obtained within 10 min (Fig. 2). It corresponds to 5.4 × 10^4 times of that of thermal equilibrium under the same conditions.

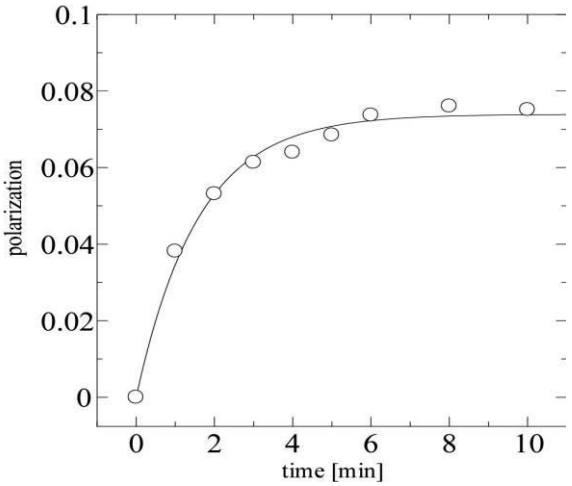

Fig. 2: Buildup of the proton polarization in 0.4 T and at room temperature. The size was 2.4 μm×0.7 mm^2. The buildup time constant 1.59 min and maximum proton polarization 0.074 were obtained by fitting the data.

The polarization is restricted by the repetition rate of our laser. The repetition rate of 50 Hz is much longer than the life time of the triplet state of 100 μs. Thus, we expect that the polarization can be increased several times using higher repetition rate optical system with preventing sample from heating. Our result and Tycko's considerations [5] suggest that overlayer materials deposited on the thin film can be detected. Moreover, our method is most likely applicable to nuclear physics [6], and initialization of quantum computer [7].

This work was supported by JST CREST, MEXT Grant-in-Aid for Scientific Research on Innovative Areas 21102004, FIRST and Global-COE .

References:

[1] A. Lesage et al., *J. Am. Chem. Soc*, 132 (2010) 15459.
[2] K. Takeda, *VDM Verlag*, (2009).
[3] A. Kagawa et al,. *J. Magn. Res*. 197 (2009) 9.
[4] S. Hashimoto et al, *Jpn. J. Appl. Phys*. 27 (1988) 726.
[5] C. Michal et al, *Phys. Rev. Lett*. 81 (1998) 3988.
[6] T. Uesaka et al, *Phys. Rev. C*, 82 (2010) 021602.
[7] A. Kagawa et al, *Rev. Sci. Instrum*., 80 (2009) 044705.